International Journal of Non-Linear Mechanics 145 (2022) 104078

Contents lists available at ScienceDirect

International Journal of Non-Linear Mechanics

journal homepage: www.elsevier.com/locate/nlm

A discussion regarding reduced-order modelling of inclined elastic and immersed cables under support excitation

Guilherme Jorge Vernizzi [a,*], Stefano Lenci [b], Guilherme Rosa Franzini [a]

[a] Offshore Mechanics Laboratory - LMO, Escola Politécnica, University of São Paulo, Brazil
[b] Università Politecnica delle Marche, Ancona, Italy

ARTICLE INFO

Keywords:
Reduced-order model
Elastic cable
Imposed boundary motion
Offshore engineering

ABSTRACT

This paper investigates the advantages or issues of different reduced-order models (ROMs) for the analysis of elastic cables hanging between two supports at different height. The cable is considered immersed in still fluid and under the action of an imposed boundary motion at the upper support. Nine ROMs are explored, obtained from the combination of three different functions responsible for ensuring the interpolation of the boundary motion with three possible sets of projection functions associated with the degrees of freedom (DOF). For the interpolation functions, the possibilities are: (i) a linear interpolation, (ii) a linear interpolation with a decomposition in axial and transversal directions according to the local angle of each cross-section, or, (iii) a quasi-static approach using the static displacement of the cable due to a unitary displacement applied at the moving boundary. Regarding the number of DOFs, the possible functions sets consists of a single mode of vibration, three modes of vibration, or, a group of five trigonometric functions. The ROMs are then simulated for different conditions and the results are compared to a reference case obtained from Finite Element Method (FEM). Additionally to the numerical analysis, a novel semi-analytical solution is proposed for the single DOF ROMs based on the method of multiple time scales (MMTS). Such solution tackles an issue of using the Morrison damping since it contains an absolute value function in its formulation which makes it unfeasible to compute the integrals that appear in the Galerkin method without knowing the response of the structure. The results show that the choice of the function to interpolate the top motion effects is of top-most importance, since a poor choice of that set of functions leads to low accuracy in the results that cannot be solved by adding more DOFs to the ROM. It is also shown that working with more complex functions instead of simple trigonometric functions leads to a significance enhancement of the computational performance of the simulations.

1. Introduction

Cables are very slender structures, presenting negligible flexural stiffness, with applications to various engineering problems. They can be found in stayed and suspended bridges, mooring systems of marine vessels and offshore platforms, or as elements to transport payloads or raw materials across long distances. Due to their slenderness, cables may present a rich behaviour under external disturbances from applied loads, motion prescribed to the support, fluid–structure interaction, soil–structure interaction, amongst others. Cases of modal coupling, internal resonances and chaotic dynamics may arise, pointing out the need for a deep understanding of the dynamical responses of this kind of structure. The first step of any such investigation is obviously the modelling of the structure. For that matter, the works in [1,2] present a detailed discussion with different modelling approaches together with suggestions of pathways for the analysis.

An initial point of a well-structured investigation about the linear free vibration problem of cables is presented in [3,4]. In those works, horizontal cables with a small sag-to-span ratio are considered, and a detailed study is made analysing the rich linear modal properties that this type of structure may present. In [5], numerical confirmations with the Finite Element Method (FEM) are obtained for the predictions made in [3]. In [6] the linear modal investigation of horizontal cables with small sag-to-span ratio is extended to the possibility of flexible supports. Following, a rich analysis of the linear free dynamics of inclined taut strings is made in [7], with an asymptotic solution presented in [8] and experimental correlations confirming the findings in [9].

Some initial works on the non-linear free vibrations and the frequency-amplitude dependency investigation are presented in [10–12]. In [13], the modal coupling between in-plane and out-of-plane modes for shallow horizontal cables under free vibrations is addressed. In turn, forced vibration considering super and subharmonic resonances are investigated in [14,15], respectively. Notice that those earlier works considered only the particular conditions of taut strings

* Corresponding author.
E-mail address: guilherme.jorge.lopes@usp.com.br (G.J. Vernizzi).

https://doi.org/10.1016/j.ijnonlinmec.2022.104078
Received 29 December 2021; Received in revised form 27 April 2022; Accepted 7 May 2022
Available online 18 May 2022

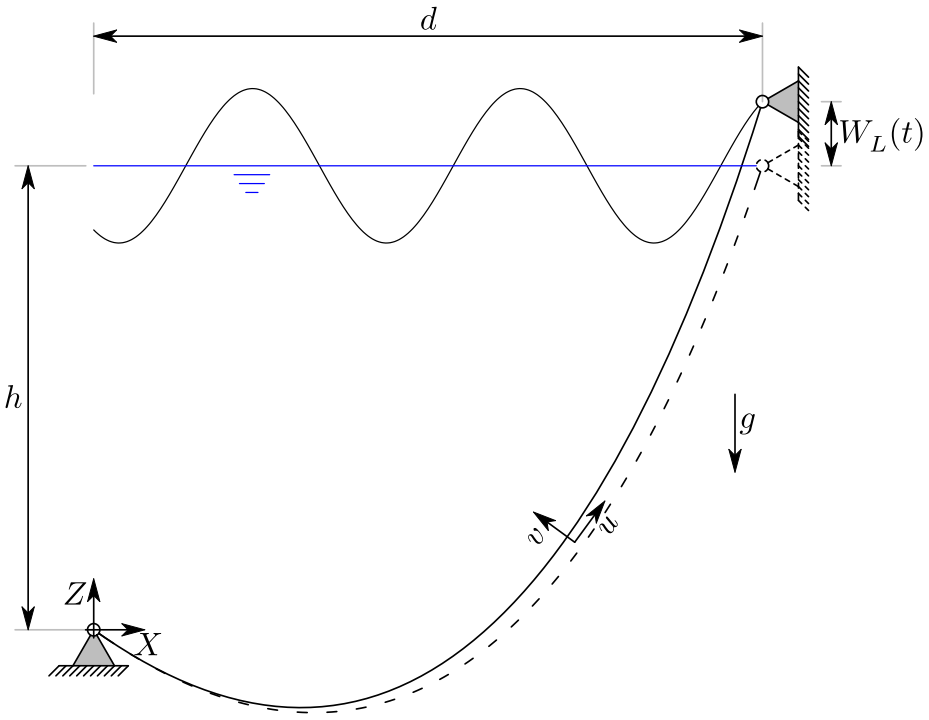

Fig. 1. Basic model.

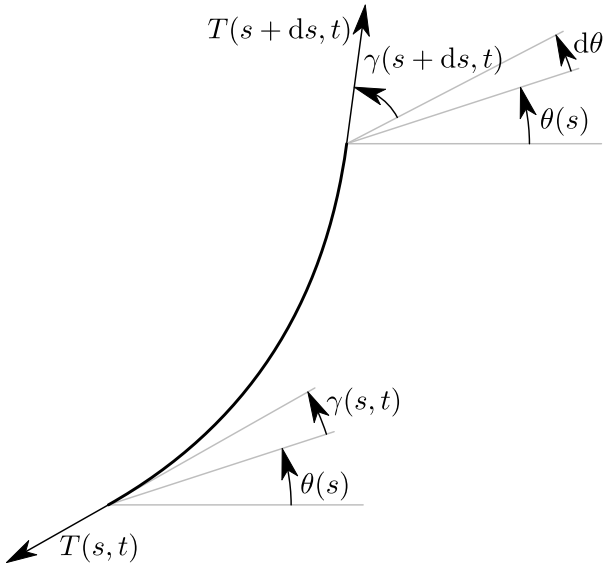

Fig. 2. Forces acting on an infinitesimal cable element.

or shallow horizontal cables. Also, there are no considerations regarding fluid–structure interactions or effects of imposed motions at the supports.

Considering a sagged and inclined configuration together with interactions with the surrounding fluid, in [16] the linear modal shapes and frequencies of a typical configuration of steel catenary risers for offshore engineering applications are obtained by means of the WKB method (see [17]). Also removing the shallow or taut cable conditions, non-linear free vibrations of arbitrarily sagged and inclined cables are investigated in [18], with modal coupling being investigated in [19]. Those studies are complemented with the analysis of 2:1 internal resonance investigations made in [20,21]. In [22], the effects of self-weight of taut inclined cables on the linear free vibrations are explored. Following, a complete discussion and classification of linear modal properties in the style of [3] is made for horizontal non-shallow cables in [23]. This type of study and classification is then extended to non-shallow inclined cables in [24]. Finally, an approximated solution for the amplitude dependent modal shapes and frequencies for inclined cables with small sag-to-span ratio is presented in [25].

Regarding the effects of imposed motion at the supports, the topic was widely introduced during the 90's, with works in shallow horizontal cables by [26–28] and also by means of experimental investigations in [29]. The arising of multiple bifurcations and chaotic dynamics is demonstrated in [30] when both external forcing and support excitations are considered. An interesting analytical approach to shallow horizontal cables under out-of-plane support imposed motion is presented in [31]. In the latter work, the support excitation is deemed small in a multiple scale expansion, in order for the imposed motion to appear only on the modulation equations, allowing for a simple modal solution of the first-order problem. The same approach is applied in [32], while also considering in-plane vertical motion of the support. In [33], non-ideal support conditions are considered by means of a lumped mass–string–damper system and it is shown how a tuning of those parameters may change the behaviour of symmetric and antisymmetric modes in the response. Asynchronicity of the imposed out-of-plane motion is introduced in [34]. The authors are able to investigate the effect of phase lag between excitations in different supports in terms of response behaviour and conditions for dynamical instabilities to arise. In [35], such analysis is extended to the case of in-plane imposed support motion with phase lag in the motion of different supports. Finally, the removal of small sag-to-span ratio is made in [36] for horizontal cables under support excitation.

For applications on inclined taut strings, a detailed pioneer work is presented in [37], containing analytical investigations by means of a solution obtained with the application of the method of multiple time scales (MMTS) directly to the partial differential equations (PDEs) of motion of the system, together with experimental correlations. Non-linear vibrations of an inclined taut string are considered in [38] together with experimental correlation. In [39], the non-planar motion of the same type of cable is investigated. Parametric instability of out-of-plane modes due to support excitation on inclined taut cables is addressed in [40]. The extension for considering both in and out-of-plane motions is made in [41] for modal instabilities of chosen modes. The extension to multi-modal analysis is then made in [42]. It is important to highlight the contribution of readily available analytical solutions presented in those works. Finally, in [43], the support excitation on a taut cable is combined with galloping induced by wind flow.

The consideration of surrounding fluid different from air is made in [44–46]. Those studies consider the in-plane dynamics of marine inclined risers without sag-to-span ratio limitations. In [44], the 2:1 internal resonances of this type of structure are addressed by using the MMTS. The same kind of analysis in then made for the 3:1 case of internal resonance in [45]. Finally, multi-frequency forcing terms are considered in [46] to emulate the fluid–structure interactions. It is important to remark, however, that none of these works considered the presence of non-linear hydrodynamic damping (quadratic in the velocity) in the formulation. The main concern is that this type of damping is of paramount importance in the dynamical response of slender structures immersed in fluid, as can be seen in [47–49].

Notice that, in the majority of the studies, an order reduction of the model is made, by considering oscillations with a single frequency or producing reduced-order models (ROMs) via a discretization procedure. However, studies regarding those methodologies themselves and how they affect the obtained results are few. Two main issues can be highlighted in the process of reduced-order modelling. The first one consists of the quantitative behaviour of the model. Usually, discretization procedures are based on projection techniques, such as the Galerkin projection, and the number of projection functions is increased until adequate adherence to some reference is achieved. The issue is that different sets of projection functions can lead to a different number of such functions to be needed in order to conceive an adequate model, as shown in [48] for vertical slender structures. It is worth noticing that the latter work shows that this effect may be significant even when the geometrical differences between projection functions are small. The second question is related to the qualitative behaviour. Although the Galerkin projection ensures that the error of the ROM will be the smallest possible with relation to the projected basis, it does not give conditions to ensure that this minimum error does not interfere with the qualitative behaviour of the system. An investigation of the effects of reducing techniques is made in [50], where theoretical comparisons and possible drawbacks are investigated for the cases of applying the MMTS directly to the PDEs of motion or formulating ordinary differential equations (ODEs) of motion after a Galerkin procedure. An analysis comparing two different perturbation approaches to the problem is made in [51].

In the presented context, the work herein proposed is to investigate the effects of using different projection basis for obtaining ROMs for inclined elastic cables, with arbitrary sag-to-span ratio, immersed in still fluid with significant non-linear dampening effect, subjected to in-plane imposed motion in the top support. The problem of performing a detailed investigation of the impacts of different projection functions goes beyond simple accuracy convergence. As mentioned, qualitative errors can occur, which cannot always be solved by simply increasing the number of projection functions. Besides, finding a minimal ROM leads to analysis advantages. Smaller models allow for easier applications of analytical methods and reduce computational effort for large simulations campaigns such as obtaining basins of attraction or performing initial design studies to choose a better tuning for certain structural properties. The main contribution is then to clarify the issues in choosing projection functions, their limitations and needed investigation for their future enhancement.

Notice that the investigation herein proposed concerns ROMs obtained via Galerkin projections. This however is not the only possibility of conceiving ROMs. Other possible ways involve, for example, the use of Proper Orthogonal Decomposition (POD), Non-linear Normal modes (NNM) and Spectral Submanifolds (SSM). Each of those methods have their own advantages and drawbacks, with the choice of which one to use depending on the particular problem and the desired analysis. The POD is a statistical method and needs a previously obtained data to be applied on. The method then furnishes the so called proper orthogonal modes (POM) which are useful to represent the data using a small amount of eigenfunctions. A detailed review on the POD with its history of research, mathematical basis and applications to structural engineering can be found in [52]. Following, the NNM are an extent of the concept of linear modes of vibration to the non-linear regime (see, for example, [53] for a detailed description). The idea is to obtain manifolds over which the dynamical response of the system can be captured with a small number of DOFs. The task however can be very complicated from a mathematical point of view, with different approaches and techniques being proposed along time, using center manifold theory [53], Galerkin approximations [54] or the MMTS [55]. For a recent review with discussions on the applications of NNMs and numerical implementation see [56,57]. For a detailed review of NNMs and comparisons with other forms to obtain ROMs see [58]. Finally, the SSM is a recent concept in non-linear dynamics, which has essential relationship to NNMs. By definition, SSMs are invariant manifolds that are the smoothest (mathematically speaking) nonlinear continuation of the spectral components along a given NNM. One of the great advantages of the SSMs is their demonstrated uniqueness given certain spectral conditions are satisfied. This uniqueness is not guaranteed in previous approaches to obtain invariant manifolds to represent NNMs. The details of the theory behind SSMs can be found in [59] together with proofs of existence and uniqueness. The application of the SSM approach to obtain ROMs for can be found in [60].

The article is divided as follows. In Section 2, the formulation of the PDEs of motion is shown considering a local reference frame. The reduced-order modelling procedure is then explained in Section 3 together with the definition of the different ROMs investigated in this work. Then, considering the simplest ROM obtained, a novel semi-analytical solution using the MMTS is presented in Section 4. The proposed ROMs are then compared with a higher-order hierarchical model based on FEM, used as reference, in Section 5, illustrating the differences between approaches. Finally, the main conclusions are summarized in Section 6.

2. Partial differential equations of motion

The structure under investigation is presented in Fig. 1, together with the relevant geometric measures and axes definition. As shown, the sag-to-span ratio is not necessarily small and the supports can be at different heights.

As depicted, X and Z are fixed Cartesian axes at the left support. The Z direction is considered to be the vertical one, with gravity acting downwards. A local frame is also defined, with u being the tangential/axial direction and v being the normal/transversal direction. The horizontal and vertical distances between supports are given by d and h respectively. For the sake of illustration, the numerical investigations carried in this work are made with a cable with 2452.46 m of length, $d = 1500$m and $h = 1800$m, leading to a non-shallow configuration. In this work, the fluid is considered to be still and the structure has negligible flexural stiffness. In order to obtain the equations of motion, consider the infinitesimal element presented in Fig. 2.

In Fig. 2, T is the tension developed in the structure, considering the effective tension concept (see [1]), θ is the angle of the local axial

direction with the Cartesian horizontal direction, γ is the increment of such an angle in the dynamical response of the structure and $\mathrm{d}\theta$ is the increment of $\theta(s)$ that occurs in the represented arc span $\mathrm{d}s$. Let F_u and F_v denote the resultant of the internal forces acting in an infinitesimal element $\mathrm{d}s$ accordingly to the axial and transversal direction respectively, considering the static configuration for those directions, with s being the arclength coordinate measured from the left support. By the geometry of the problem, those resultants are written as

$$F_u = T\left(s+\mathrm{d}s\right)\cos\left(\mathrm{d}\theta+\gamma\left(s+\mathrm{d}s\right)\right) - T\left(s\right)\cos\left(\gamma\left(s\right)\right), \tag{1}$$

$$F_v = T\left(s+\mathrm{d}s\right)\sin\left(\mathrm{d}\theta+\gamma\left(s+\mathrm{d}s\right)\right) - T\left(s\right)\sin\left(\gamma\left(s\right)\right). \tag{2}$$

The external forces acting on the element are the net weight (weight minus buoyancy force) and those resulting from the fluid–structure interaction. For the latter case, the Morrison non-linear damping is considered together with the potential added mass. For the non-linear damping, the direction transversal to each cross-section is taken as the direction v defined in the static configuration. This is an approximation since the instantaneous transversal direction is, in general, different from the one in the static configuration. However, this approximation is suitable while the dynamic displacements around the static configuration are small compared to the wave-length of the vibration modes with significant participation in the motion. The assumption that this occurs in the present case is even more suitable considering that this type of damping significantly reduces the magnitude of the oscillations. Now, writing Newton's second law for the infinitesimal element leads to

$$F_u - \gamma_s \mathrm{d}s\sin\theta = m\ddot{u}\mathrm{d}s, \tag{3}$$

$$F_v - \gamma_s \mathrm{d}s\cos\theta - \frac{1}{2}\rho D\overline{C}_D\dot{v}\left|\dot{v}\right|\mathrm{d}s = m_t\ddot{v}\mathrm{d}s, \tag{4}$$

where γ_s is the immersed weight per unit length, ρ is the specific mass of the surrounding fluid, D is the structural diameter of the cable, assumed as having a circular cross-section, $\overline{C}_D$ is the mean drag coefficient, m is the mass per unit length of the cable and m_t is the mass per unit length summed up with the potential added mass. Notice that the tangential added mass is not considered in the formulation, provided it is much smaller than its transversal counterpart. As usual in the literature, overdots are used to denote differentiation with respect to time. To obtain the equations of motion, both Eqs. (3) and (4) are divided by $\mathrm{d}s$ and the limit is taken for $\mathrm{d}s \mapsto 0$. For the resultants F_u and F_v it follows that

$$\begin{aligned}
&\lim_{\mathrm{d}s\mapsto 0}\frac{F_u}{\mathrm{d}s} = \\
&\lim_{\mathrm{d}s\mapsto 0}\frac{T\left(s+\mathrm{d}s\right)\cos\left(\mathrm{d}\theta+\gamma\left(s+\mathrm{d}s\right)\right) - T\left(s\right)\cos\left(\gamma\left(s\right)\right)}{\mathrm{d}s} = \\
&\lim_{\mathrm{d}s\mapsto 0}\frac{T\left(s+\mathrm{d}s\right)\cos\left(\gamma\left(s+\mathrm{d}s\right)\right) - T\left(s\right)\cos\left(\gamma\left(s\right)\right)}{\mathrm{d}s} \\
&- \frac{T\left(s+\mathrm{d}s\right)\sin\left(\gamma\left(s+\mathrm{d}s\right)\right)\mathrm{d}\theta + O(\mathrm{d}\theta^2)}{\mathrm{d}s} = \\
&T'\cos\gamma - T\left(\theta'+\gamma'\right)\sin\gamma,
\end{aligned} \tag{5}$$

$$\begin{aligned}
&\lim_{\mathrm{d}s\mapsto 0}\frac{F_v}{\mathrm{d}s} = \\
&\lim_{\mathrm{d}s\mapsto 0}\frac{T\left(s+\mathrm{d}s\right)\sin\left(\mathrm{d}\theta+\gamma\left(s+\mathrm{d}s\right)\right) - T\left(s\right)\sin\left(\gamma\left(s\right)\right)}{\mathrm{d}s} = \\
&\lim_{\mathrm{d}s\mapsto 0}\frac{T\left(s+\mathrm{d}s\right)\sin\left(\gamma\left(s+\mathrm{d}s\right)\right) - T\left(s\right)\sin\left(\gamma\left(s\right)\right)}{\mathrm{d}s} \\
&+ \frac{T\left(s+\mathrm{d}s\right)\cos\left(\gamma\left(s+\mathrm{d}s\right)\right)\mathrm{d}\theta + O(\mathrm{d}\theta^2)}{\mathrm{d}s} = \\
&T'\sin\gamma + T\left(\theta'+\gamma'\right)\cos\gamma.
\end{aligned} \tag{6}$$

Differentiation with respect to s is denoted by primes. The notation $O(\mathrm{d}\theta^2)$ means terms of order equal to or higher than $\mathrm{d}\theta^2$. Notice that this usage does not imply an approximation since those terms are indeed null when the limit is taken. Let now the tension to be divided as $T = T_s + T_d$ with T_s being the tension in the static configuration and T_d any variation over it after the structure starts oscillating. With that division, the equations for planar motion written in the static configuration reference frame read

$$\begin{aligned}
&\left(T_s'+T_d'\right)\cos\gamma - \left(T_s+T_d\right)\left(\theta'+\gamma'\right)\sin\gamma \\
&- \gamma_s\sin\theta = m\ddot{u},
\end{aligned} \tag{7}$$

$$\begin{aligned}
&\left(T_s'+T_d'\right)\sin\gamma + \left(T_s+T_d\right)\left(\theta'+\gamma'\right)\cos\gamma - \gamma_s\cos\theta \\
&= \frac{1}{2}\rho D\overline{C}_D\dot{v}\left|\dot{v}\right| + m_t\ddot{v}.
\end{aligned} \tag{8}$$

The static equilibrium of the cable may be recognized in Eqs. (7) and (8) by setting $T_d = \gamma = 0$ as well as ruling out the time derivatives. This leads to the expressions

$$T_s' - \gamma_s\sin\theta = 0, \tag{9}$$

$$T_s\theta' - \gamma_s\cos\theta = 0. \tag{10}$$

Notice that the expressions for the static equilibrium are exactly the same as for the case of the inextensible cable. The difference is that, in the former, the unknowns of the problem are T_s and θ, while for the extensible case one must use the constitutive and compatibility relationships to write T_s and θ in terms of the unknown static configuration and then solve the problem of finding the two functions necessary to describe such configuration. The advantage in isolating the static equilibrium is that it may be solved beforehand, either analytically or numerically, allowing to reduce the equations of motion to

$$\begin{aligned}
&T_s'\left(\cos\gamma - 1\right) - T_s\left(\theta'+\gamma'\right)\sin\gamma + T_d'\cos\gamma \\
&- T_d\left(\theta'+\gamma'\right)\sin\gamma = m\ddot{u},
\end{aligned} \tag{11}$$

$$\begin{aligned}
&T_s'\sin\gamma - T_s\theta' + T_s\left(\theta'+\gamma'\right)\cos\gamma + T_d'\sin\gamma \\
&+ T_d\left(\theta'+\gamma'\right)\cos\gamma - \frac{1}{2}\rho D\overline{C}_D\dot{v}\left|\dot{v}\right| = m_t\ddot{v}.
\end{aligned} \tag{12}$$

Now, in order to simplify the model, it is assumed that the deformations are small, such that the total strain may be written as $\varepsilon \approx \varepsilon_s + \varepsilon_d$, with ε_s being the linear strain in the static configuration and ε_d the linear strain due to the displacements u and v. By definition, the linear strain ε_d is related to its correspondent quadratic Green strain ε_q by

$$1 + \varepsilon_d = \sqrt{1+2\varepsilon_q}. \tag{13}$$

Using now some laborious differential geometry calculations and the strain definitions for material curves [61], it is find that the quadratic strain is given by

$$\varepsilon_q = \left(u' - \left(v - uv' + u'v\right)\theta' + \frac{\left(u'^2 + v'^2 + \left(u\theta'\right)^2 + \left(v\theta'\right)^2\right)}{2}\right). \tag{14}$$

In addition, the angle γ is obtained from geometric relations as

$$\sin\gamma = \frac{\left(u\theta'+v'\right)}{\left(1+\varepsilon_d\right)}, \tag{15}$$

$$\cos\gamma = \frac{\left(1+u'-v\theta'\right)}{\left(1+\varepsilon_d\right)}, \tag{16}$$

$$\gamma = \arcsin\left(\frac{\left(u\theta'+v'\right)}{\left(1+\varepsilon_d\right)}\right). \tag{17}$$

Following [1], disregarding the Poisson effect, the effective tension is given by

$$T = EA\varepsilon + p_e A, \tag{18}$$

where p_e is the external fluid pressure and no internal fluid is considered in the cable. Defining the depth of a cable element in the static configuration as h_s, the external pressure is written as

$$p_e = \rho g \left(h_s - u \sin\theta - v \cos\theta\right). \tag{19}$$

Recalling the decomposition of the tension in statical and dynamical components, it is obtained that

$$T_s + T_d = \left(EA\varepsilon_s + \rho g A h_s\right) + \left(EA\varepsilon_d - \rho g A \left(u \sin\theta + v\cos\theta\right)\right), \tag{20}$$

which leads to

$$T_d = EA\varepsilon_d - \rho g A \left(u \sin\theta + v \cos\theta\right). \tag{21}$$

From Eq. (17) it is obtained that

$$\gamma' = \frac{1}{\cos\gamma}\left(\frac{\left(u\theta' + v'\right)}{\left(1+\varepsilon_d\right)}\right)' = \frac{\left(1+\varepsilon_d\right)}{\left(1+u'-v\theta'\right)}\left(\frac{\left(u\theta'+v'\right)}{\left(1+\varepsilon_d\right)}\right)'. \tag{22}$$

Substituting now Eqs. (15) to (22) in (11) and (12), the equations of motion are given as

$$\begin{aligned}
&T_s'\left(\frac{u'-v\theta'-\varepsilon_d}{1+\varepsilon_d}\right) + EA\varepsilon_d' \frac{\left(1+u'-v\theta'\right)}{\left(1+\varepsilon_d\right)} \\
&- T_s\left(\frac{\left(u\theta'+v'\right)\theta'}{\left(1+\varepsilon_d\right)} + \frac{\left(u\theta'+v'\right)}{\left(1+u'-v\theta'\right)}\left(\frac{\left(u\theta'+v'\right)}{\left(1+\varepsilon_d\right)}\right)'\right) \\
&- \rho g A\left(\left(u'-v\theta'\right)\sin\theta + \left(v'+u\theta'\right)\cos\theta\right)\frac{\left(1+u'-v\theta'\right)}{\left(1+\varepsilon_d\right)} \\
&+ \left[\left(\frac{\left(u\theta'+v'\right)\theta'}{\left(1+\varepsilon_d\right)} + \frac{\left(u\theta'+v'\right)}{\left(1+u'-v\theta'\right)}\left(\frac{\left(u\theta'+v'\right)}{\left(1+\varepsilon_d\right)}\right)'\right)\left(-EA\varepsilon_d\right.\right. \\
&\left.\left. + \rho g A u \sin\theta + \rho g A v \cos\theta\right)\right] - m\ddot{u} = 0,
\end{aligned} \tag{23}$$

$$\begin{aligned}
&T_s'\frac{\left(u\theta'+v'\right)}{\left(1+\varepsilon_d\right)} - T_s\theta' + EA\varepsilon_d'\frac{\left(u\theta'+v'\right)}{\left(1+\varepsilon_d\right)} \\
&+ T_s\left(\frac{\left(1+u'-v\theta'\right)\theta'}{\left(1+\varepsilon_d\right)} + \left(\frac{\left(u\theta'+v'\right)}{\left(1+\varepsilon_d\right)}\right)'\right) \\
&- \rho g A\left(\left(u'-v\theta'\right)\sin\theta + \left(v'+u\theta'\right)\cos\theta\right)\frac{\left(u\theta'+v'\right)}{\left(1+\varepsilon_d\right)} \\
&+ \left[\left(\frac{\left(1+u'-v\theta'\right)\theta'}{\left(1+\varepsilon_d\right)} + \left(\frac{\left(u\theta'+v'\right)}{\left(1+\varepsilon_d\right)}\right)'\right)\left(EA\varepsilon_d - \rho g A u \sin\theta\right.\right. \\
&\left.\left. - \rho g A v \cos\theta\right)\right] - \frac{1}{2}\rho D\overline{C}_D\dot{v}\left|\dot{v}\right| - m_t\ddot{v} = 0.
\end{aligned} \tag{24}$$

The equations of motion written as in Eqs. (23) and (24) are suitable for being put in operator form as

$$\mathscr{L}_u(u,v) = 0, \tag{25}$$

$$\mathscr{L}_v(u,v) = 0. \tag{26}$$

For further applications, all the required calculations are made considering terms up to cubic order in u and v with the aid of symbolic computation software to collect these terms.

3. Reduced-order modelling approaches

Different approaches may be applied in order to solve the equations of motion and obtain the dynamical response of the structure. One of such approaches is the use of reduced-order models obtained via transforming the system of partial differential equations into a system of ODEs. For this purpose, the Galerkin method is particularly useful given its formal simplicity while guaranteeing the smallest possible error within the projection space adopted. It requires a set of projection functions that satisfy the essential boundary conditions of the original problem. Although this is usually straightforward to ensure for problems where the essential boundary conditions are constant values, some issues may appear in the case when those boundary conditions are time-dependent, which are discussed along this work. Initially, in order to ensure that the essential boundary conditions are obeyed, the projections basis investigated obey the general formulas

$$u = W_L(t)\,\phi_s(s) + \sum_{k=1}^{n} A_k(t)\,\phi_k(s), \tag{27}$$

$$v = W_L(t)\,\psi_s(s) + \sum_{k=1}^{n} B_k(t)\,\psi_k(s). \tag{28}$$

Within this proposition, ϕ_s and ψ_s are projection functions responsible for representing the effect of the moving boundary in the axial and transversal directions, respectively. Hence, it is necessary that $\phi_s(L) = \sin\theta_L$ and $\psi_s(L) = \cos\theta_L$, with θ_L being the angle the cable axis makes with the horizontal direction in the static configuration. In turn, the functions ϕ_k and ψ_k must obey the fixed boundary conditions $\phi_k(0) = \phi_k(L) = \psi_k(0) = \psi_k(L) = 0$. The problem is then how to define the behaviour of ϕ_s and ψ_s along the structural length since no explicit conditions about them are posed by the method itself. It is also worth noticing that these functions will generate forcing terms in the equations of the ROM, and these resulting terms vary according to the selected shape functions.

The problem at hand now is how to choose suitable functions. Naturally, the best choice would be a set of functions that generates the exact solutions of the PDEs given in Eqs. (23) and (24). This solution, however, is not available, leading to the necessity of evaluating which set of functions will present a better representation of said solution, which again is the main objective of this paper. Another possibility would be to apply the MMTS directly to the PDEs of motion, as done in [49] for a straight rod. This task however is out of the scope of the present work and would generate an entire work of its own. As a final possible approach, the choice of functions can be inspired in the ones employed in similar problems and that furnished suitable results (see [43,48] for instance). In the present work, three different approaches are made for the functions ϕ_s and ψ_s. The first option is to use a simple linear interpolation of the imposed motion along the length, that is,

$$\phi_{s,1} = \left(\frac{s}{L}\right)\sin\theta_L, \tag{29}$$

$$\psi_{s,1} = \left(\frac{s}{L}\right)\cos\theta_L. \tag{30}$$

The motivation for this trial is that the linear interpolation is a good interpolation for straight vertical structures subjected to imposed motion at one support while keeping a simple expression for it (See [48], where a linear interpolation is implicit in the equations as consequence of a static condensation). The second set of trial functions for the imposed motion interpolation is to linearly interpolate the imposed motion along the length and then project it to each direction according to the local angle. This differs from the first option in the sense that the decomposition of the imposed motion in the axial and transversal directions is made for each cross section. This is a small *ansatz* over the previous set of functions, in which the effect of the local angle of the structure's axis is taken into account but still keeping a simple expression. It is important to recall that it is desirable to obtain the simplest possible ROM, which motivates the trial of using simpler expressions. The resulting functions are then

$$\phi_{s,2} = \left(\frac{s}{L}\right)\sin\theta, \tag{31}$$

$$\psi_{s,2} = \left(\frac{s}{L}\right)\cos\theta. \tag{32}$$

Finally, the third possibility herein investigated is to use a quasi-static approach to obtain the functions ϕ_s and ψ_s. This approach is used in [43] and considers that the desired functions are the difference between two static configurations. The quasi-static approach is implicit in [48], being it a result of a static condensation procedure applied to the axial dynamics. The results obtained in the latter work shows that, at least for straight structures, such approach leads to good results.

The process of obtaining the desired functions in the present case consist of applying an unitary displacement in the direction of the imposed motion and then compute the static configuration of the cable in this new boundary condition. It is assumed that this change happens almost instantaneously in the dynamic case. Obviously, this approach can only furnish readily useable expressions in particular cases such as taut cables, near parabolic cables or near inextensible catenary cables. Other applications require the problem to be solved by numeric means, which however does not pose any meaningful obstacle for the methodology itself. Considering then $X_1(s)$ and $Z_1(s)$ to be, respectively, the horizontal and vertical coordinates of the cable points after a unitary displacement is applied in the imposed motion direction, recalling that $\theta(s)$ is the correspondent angle of the cable axis with the horizontal direction. The top motion interpolation functions are given as

$$\phi_{s,3} = \left(X_1 - X_0\right)\cos\theta + \left(Z_1 - Z_0\right)\sin\theta, \tag{33}$$

$$\psi_{s,3} = -\left(X_1 - X_0\right)\sin\theta + \left(Z_1 - Z_0\right)\cos\theta. \tag{34}$$

Now, the next step is to define a set for the trial functions ϕ_k and ψ_k. Since the main goal of this paper is to show how different projection functions impact the obtained ROM, three different sets are defined. The first set, herein called 'set(i)' consists of a single mode of vibration of the structure, obtained directly from the PDEs of motion. This option is attractive since, if deemed accurate, is the smallest possible ROM, which results in the smallest mathematical and computational efforts for any subsequent analysis. Notice that, since the vibration modes of curved structures have coupled components u and v, it results that $A_k = B_k$ in Eqs. (27) and (28). Thus, the ROM with set(i) contains only one DOF. Following, considering that more modal functions may be needed for a good representation of the dynamics of the problem, set(ii) consists of three modes of vibration, also obtained directly from the PDEs of motion, thus generating a 3-DOF ROM.

Finally, one could want to use simpler functions to build the projection base, specially if those functions present a closed-form formula. In that sense, trigonometric functions are commonly used in this kind of application and will then be the kind of function to compose set(iii). The use of trigonometric functions as basis for structures which the actual modes of vibration are not trigonometric can also be seen in [48], where is also shown that the number of projection functions for an adequate result results larger than when using the actual modes of vibration for the case of straight structures. In this case, the amplitudes of each function are let independent, that is $A_k \neq B_K$, and five functions are used for each direction as

$$\phi_k = \psi_k = \sin\left(\frac{k\pi s}{L}\right), \quad k = 1, \ldots, 5. \tag{35}$$

With all the sets properly defined and chosen, it is possible to proceed with the Galerkin projection. The equations of motion, as written in Eqs. (25) and (26), leads to a vectorial equation of the form

$$\left[\mathscr{L}_u(u,v), \mathscr{L}_v(u,v)\right] = [0,0]. \tag{36}$$

The application of the Galerkin scheme for sets (i) and (ii) leads to equations of the form

$$\left\langle \left[\mathscr{L}_u(u,v), \mathscr{L}_v(u,v)\right], \left[\phi_k, \psi_k\right] \right\rangle = 0, \tag{37}$$

for each projection mode k, where $\langle , \rangle$ denotes the inner product between the left and right side. In turn, for set (iii), since the projection in each direction is assumed as independent, 5 pairs of equations are obtained as

$$\left\langle \left[\mathscr{L}_u(u,v), \mathscr{L}_v(u,v)\right], \left[\phi_i, 0\right] \right\rangle = 0, \tag{38}$$

$$\left\langle \left[\mathscr{L}_u(u,v), \mathscr{L}_v(u,v)\right], \left[0, \phi_i\right] \right\rangle = 0. \tag{39}$$

The resulting ODE of motion for set (i) is then given as

$$\begin{aligned} m_1\ddot{A}_1 &= m_q\ddot{W}_L + a_1A_1 + a_2W_L + a_3A_1^2 + a_4A_1W_L + a_5W_L^2 \\ &+ a_6A_1^3 + a_7A_1^2W_L + a_8A_1W_L^2 + a_9W_L^3 \\ &- \zeta\int_0^L \psi_1\left|\psi_1\dot{A}_1 + \psi_s\dot{W}_L\right|\left(\psi_1\dot{A}_1 + \psi_s\dot{W}_L\right)\mathrm{d}s, \end{aligned} \tag{40}$$

where m_1, m_q and the a_i's are constants resulting of the evaluation of the Galerkin integrals over the length of the structure when performing the inner product in Eq. (37). In addition, ζ is simply defined as $\zeta = \rho D\overline{C}_D/2$. Notice that, since the amplitude associated with the projection mode is unknown at this point, the integral involving the non-linear Morrison damping cannot be solved beforehand. Instead, this integral must be calculated on every single step of a numerical simulation. Following, each equation k of the ROM obtained with set (ii) is given as

$$\begin{aligned} \left(\sum_i^3 m_{k,i}\ddot{A}_i\right) &= m_{k,q}\ddot{W}_L + \left(\sum_i^3 a_{k,i}A_i\right) + a_{k,q}W_L + b_{k,q}W_L^2 \\ &+ \left(\sum_i^3 b_{k,i}W_LA_i\right) + \left(\sum_i^3\sum_j^3 b_{k,i,j}A_iA_j\right) + c_{k,q}W_L^3 \\ &+ \left(\sum_i^3 c_{k,i}W_L^2A_i\right) + \left(\sum_i^3\sum_j^3 c_{k,i,j}W_LA_iA_j\right) \\ &+ \left(\sum_i^3\sum_j^3\sum_l^3 c_{k,i,j,l}A_iA_jA_l\right) \\ &- \zeta\int_0^L \psi_k\left|\left(\sum_i^3\psi_i\dot{A}_i\right) + \psi_s\dot{W}_L\right|\left(\left(\sum_i^3\psi_i\dot{A}_i\right) + \psi_s\dot{W}_L\right)\mathrm{d}s, \end{aligned} \tag{41}$$

as in the previous case, $m_{k,i}$, $m_{k,q}$ and the a's, b's and c's are constants resulting of performing the inner product in Eq. (37). It is possible to notice that a small increase in the number of projection functions leads to a significant increase in the number of terms in each equation, as well as it considerably increases the number of integrals to be evaluated at each time-step of simulation.

4. Semi-analytical solution for particular models

As it can be seen from the equations governing the ROMs, the search for analytical solutions can be a troublesome task due to the non-linear damping. This is due the impossibility of solving the integral involving the absolute value function without knowing the solution of the problem. However, an iterative approach may be applied as it is shown here. For that, only the smallest ROM is considered, that is, the one given by Eq. (40). The equations are scaled in a way that all the constants a_i of terms involving W_L, or non-linear terms involving A_1 are mapped as

$$a_i \mapsto \epsilon a_i, \tag{42}$$

with ϵ being a small bookkeeping parameter. The solutions are then sought in the expansion form

$$A_1 = A_{1,0}\left(t_0, t_1\right) + \epsilon A_{1,1}\left(t_0, t_1\right), \tag{43}$$

with t_0 and t_1 being two time scales defined as $t_i = \epsilon^i t$. These definitions lead to differential operators for the time differentiation that can be written as

$$\frac{\mathrm{d}}{\mathrm{d}t} = \frac{\partial}{\partial t_0} + \epsilon\frac{\partial}{\partial t_1} = D_0 + \epsilon D_1, \tag{44}$$

$$\frac{\mathrm{d}^2}{\mathrm{d}t^2} = \frac{\partial^2}{\partial t_0^2} + 2\epsilon\frac{\partial^2}{\partial t_0\partial t_1} = D_0^2 + 2\epsilon D_0D_1, \tag{45}$$

both correct up to terms of order ϵ. Applying the differential operators in Eq. (40), using the trial proposed solution in Eq. (43) and then collecting terms of the same order in ϵ, two equations are obtained, being them the equation of order ϵ^0:

$$m_1D_0^2A_{1,0} - a_1A_{1,0} = 0, \tag{46}$$

and the equation of order ϵ^1:

$$m_1D_0^2A_{1,1} - a_1A_{1,1} = -2m_1D_0D_1A_{1,0} + m_q\ddot{W}_L + a_2W_L$$

$$+ a_3 A_{1,0}^2 + a_4 A_{1,0} W_L + a_5 W_L^2 + a_6 A_{1,0}^3 + a_7 A_{1,0}^2 W_L + a_8 A_{1,0} W_L^2 + a_9 W_L^3 - \zeta \int_0^L \psi_1 \left|\psi_1 D_0 A_{1,0} + \psi_s D_0 W_L\right| \left(\psi_1 D_0 A_{1,0} + \psi_s D_0 W_L\right) \mathrm{d}s. \quad (47)$$

From Eq. (46), the solution for $A_{1,0}$ is simply given as

$$A_{1,0} = B_0 e^{i\omega_0 t_0} + B_0^* e^{-i\omega_0 t_0} = B_0 e^{i\omega t_0} + c.c., \quad (48)$$

where i is the imaginary constant, ω_0 is the natural frequency of the obtained linear oscillator with $\omega_0 = \sqrt{a_1/m_1}$, * denotes the complex conjugate of a term and $c.c.$ stands for the complex conjugate of all the terms before it. The case of 1:1 resonance between the structure and the imposed motion is now considered. Let then $W_L = \eta \sin(\omega_0 t_0)$. No detuning is herein considered since it hinders the capability of directly obtaining the steady-state regime amplitude for this particular problem. The extension of this analysis by means of further application of other approximation techniques is thus a suggestion for future works. Now, substituting the solution for $A_{1,0}$ in Eq. (47) leads to

$$\begin{aligned} &m_1 D_0^2 A_{1,1} - a_1 A_{1,1} = -2im_1\omega_0 D_1 B_0 e^{i\omega_0 t_0} \\ &+ \left(\frac{im_q\omega_0^2\eta}{2} - \frac{ia_2\eta}{2}\right) e^{i\omega_0 t_0} + a_3\left(B_0^2 e^{2i\omega_0 t_0} + B_0 B_0^*\right) \\ &- \frac{ia_4\eta}{2}\left(B_0 e^{2i\omega_0 t_0} - B_0\right) - \frac{a_5\eta^2}{4}\left(e^{2i\omega_0 t_0} - 1\right) \\ &+ a_6\left(B_0^3 e^{3i\omega_0 t_0} + 3B_0^2 B_0^* e^{i\omega_0 t_0}\right) \\ &- \frac{ia_7\eta}{2}\left(B_0^2 e^{3i\omega_0 t_0} + \left(-B_0^2 + 2B_0 B_0^*\right) e^{i\omega_0 t_0}\right) \\ &- \frac{a_8\eta^2}{4}\left(B_0 e^{3i\omega_0 t_0} + \left(B_0^* - 2B_0\right) e^{i\omega_0 t_0}\right) \\ &+ \frac{ia_9\eta^3}{8}\left(e^{3i\omega_0 t_0} - 3e^{i\omega_0 t_0}\right) + c.c. \\ &- \zeta \int_0^L \psi_1 \left|\psi_1 D_0 A_{1,0} + \psi_s D_0 W_L\right| \left(\psi_1 D_0 A_{1,0} + \psi_s D_0 W_L\right) \mathrm{d}s. \end{aligned} \quad (49)$$

The compatibility condition is then given by requiring that the term on the right-hand side does not belong to the kernel of the operator at the left-hand side of the equation, which is analogous to require that the forcing term is non-resonant with the oscillator given by the left side in the case of ODE. To this end, the terms with frequency ω_0 must vanish, leading to

$$-2im_1\omega_0 D_1 B_0 + \frac{im_q\omega_0^2\eta}{2} - \frac{ia_2\eta}{2} + 3a_6 B_0^2 B_0^* + \frac{ia_7}{2}\eta B_0^2 - ia_7\eta B_0 B_0^* + \frac{a_8}{2}\eta^2 B_0 - \frac{a_8}{4}\eta^2 B_0^* - \frac{3ia_9}{8}\eta^3 + F_0 = 0, \quad (50)$$

with F_0 standing for any components of the non-linear damping that can lead to terms with frequency ω_0, still to be determined. In order to determine those terms, the unsolved integral is split as

$$\begin{aligned} &\int_0^L \psi_1 \left|\psi_1 D_0 A_{1,0} + \psi_s D_0 W_L\right| \left(\psi_1 D_0 A_{1,0} + \psi_s D_0 W_L\right) \mathrm{d}s = \\ &D_0 A_{1,0} \int_0^L \psi_1^2 \left|\psi_1 D_0 A_{1,0} + \psi_s D_0 W_L\right| \mathrm{d}s \\ &+ D_0 W_L \int_0^L \psi_1\psi_s \left|\psi_1 D_0 A_{1,0} + \psi_s D_0 W_L\right| \mathrm{d}s. \end{aligned} \quad (51)$$

In such way, a Fourier series expansion is applied to each integral, following the suggestions in [62], allowing to express them as

$$\int_0^L \psi_1^2 \left|\psi_1 D_0 A_{1,0} + \psi_s D_0 W_L\right| \mathrm{d}s = \sum_j \left(f_j e^{ij\omega_0 t_0} + c.c.\right), \quad (52)$$

and

$$\int_0^L \psi_1\psi_s \left|\psi_1 D_0 A_{1,0} + \psi_s D_0 W_L\right| \mathrm{d}s = \sum_j \left(g_j e^{ij\omega_0 t_0} + c.c.\right). \quad (53)$$

Applying those results in Eq. (49) and noticing that terms of frequency ω_0 are generated by the components of those integrals with frequencies 0 and $2\omega_0$ leads to

$$F_0 = -\zeta\left(i\omega_0 f_0 B_0 - i\omega_0 f_2 B_0^* + \frac{\omega_0 g_0\eta + \omega_0 g_2\eta}{2}\right). \quad (54)$$

It is important to notice that, while f_0 and g_0 are certainly real valued parameters, both f_2 and g_2 can be complex, so it is convenient to define them as $f_2 = f_{2r} + if_{2c}$ and $g_2 = g_{2r} + ig_{2c}$. Focus is now placed in obtaining stationary solutions, that is, $D_1^0 B_0^0 = 0$. Considering then the polar decomposition $B_0 = R_0 e^{i\varphi}$, the compatibility condition given by Eq. (50) can be decomposed in its real and imaginary parts, leading to the system of equations

$$\begin{aligned} &-\frac{\omega_0^2\eta m_q}{2}\sin\varphi + \frac{a_2\eta}{2}\sin\varphi + \zeta\omega_0 f_{2r} R_0 \sin 2\varphi \\ &- \zeta\omega_0 f_{2c} R_0 \cos 2\varphi - \frac{\zeta\omega_0 g_0\eta}{2}\cos\varphi - \frac{\zeta\omega_0 g_{2r}\eta}{2}\cos\varphi \\ &- \frac{\zeta\omega_0 g_{2c}\eta}{2}\sin\varphi = 0 \end{aligned} \quad (55)$$

$$\begin{aligned} &-\frac{\omega_0^2\eta m_q}{2}\cos\varphi + \frac{a_2\eta}{2}\cos\varphi - \zeta\omega_0 f_0 R_0 \\ &+ \zeta\omega_0 f_{2r} R_0 \cos 2\varphi + \zeta\omega_0 f_{2c} R_0 \sin 2\varphi + \frac{\zeta\omega_0 g_0\eta}{2}\sin\varphi \\ &+ \frac{\zeta\omega_0 g_{2r}\eta}{2}\sin\varphi - \frac{\zeta\omega_0 g_{2c}\eta}{2}\cos\varphi = 0 \end{aligned} \quad (56)$$

The problem that now arises is to evaluate the constants f_0, f_2, g_0, and g_2 without yet finding the final solution of $A_{1,0}$. To do so, an iterative numeric scheme is now proposed. The constants can be readily evaluated if the condition $A_{1,0} = 0$ is considered. Once there constants are evaluated, Eqs. (55) and (56) can be solved to obtain values for R_0 and φ. With these quantities, the new value of $A_{1,0}$ is computed and the constants f_0, f_2, g_0, and g_2 can be re-evaluated. The process can then be repeated until convergence is achieved for the values of R_0 and φ. Notice that, in order to obtain the steady-state response for different values of η, the results can be calculated in an incremental fashion. To apply this idea, one can use the result for the previous case as initial guess instead of starting from $A_{1,0}$ for each new value of η, thus reducing the necessary computational time to converge to the new solution.

5. Comparison between approaches

Aiming at illustrating the differences between the studied approaches for the ROM conception without restricting the study to specific simplified cases, an example of an inclined cable with significant sag is investigated. The results are compared to numerical solutions obtained from FEM. For that, the in-house software Giraffe [63] is used. Amongst other usages, Giraffe has been successfully employed for dynamical analysis of catenary risers. The submerged weight, added mass and Morrison drag forces are implemented in the software with the same hypotheses used in the mathematical modelling herein presented, reducing the sources of possible discrepancies between the ROMs and the FEM simulations. Another important feature is that Giraffe allows for the imposed motion at the top end to be applied as a prescribed displacement varying with time, which also matches the modelling hypothesis adopted for the ROMs. The formulation of the elements used in Giraffe for the present example is presented in [64]. Further details regarding the software's usage and analysis capabilities can be found in [63,65].

Consider then a cable with horizontal and vertical distances between supports of 1500 m and 1800 m respectively. The relevant structural data and hydrodynamic parameters are shown in Table 1.

Table 1
Structural and hydrodynamical properties for the model.

Property	Description	Value
μ	Mass per length	108 kg/m
γ_s	Immersed weight per length	727 N/m
EA	Axial stiffness	2314.0×10^6 N
L	Length	2452.46 m
ρ	Fluid density	1025 kg/m^3
D	Structural diameter	0.2032 m
$\overline{C}_D$	Mean drag coefficient	1.2000
C_a	Added mass coefficient	1.0737

Table 2
Comparison of the natural frequencies obtained for the structure considering the FEM or a direct obtaining from the PDEs.

Mode	Model	Freq. [rad/s]	Rel. diff. %
1	FEM	0.1983	–
1	PDE	0.1998	0.76
2	FEM	0.3147	–
2	PDE	0.3167	0.64
3	FEM	0.4402	–
3	PDE	0.4431	0.66
4	FEM	0.5522	–
4	PDE	0.5557	0.63
5	FEM	0.6719	–
5	PDE	0.6762	0.64

Table 3
Comparison of the natural frequencies obtained for the structure considering the FEM and the ROMs.

Mode	Model	Freq. [rad/s]	Rel. diff. %
1	FEM	0.1983	–
1	ROM(i)	0.1996	0.66
1	ROM(ii)	0.1995	0.61
1	ROM(iii)	0.1885	−4.94
2	FEM	0.3147	–
2	ROM(i)	–	–
2	ROM(ii)	0.3170	0.76
2	ROM(iii)	0.3351	6.48
3	FEM	0.4402	–
3	ROM(i)	–	–
3	ROM(ii)	0.4435	0.76
3	ROM(iii)	0.5610	27.44

With the presented data the static configuration is shown in Fig. 3, where it can be confirmed that the case in consideration does not assume simplified conditions such as small sag.

In order to validate the presented mathematical model, the natural frequencies obtained with the FEM are compared to those obtained using the native PDE eigensystem solver of Mathematica® applied to the presented equations of motion in Table 2. Complementing the result, the natural frequencies obtained with the ROMs are compared with the FEM result in Table 3. The native solver of Mathematica® uses an internal finite element scheme to discretize the furnished equations in the domain and then solves for the eigenvalues and eigenvectors for the obtained discretized system. The maximum length of the element in the solver for this case was set as 10m, since further refinement did not impact on the obtained frequencies. The convergence of the natural frequencies using the Mathematica® solver is shown by the data in Table 4. Regarding the FEM used within the Giraffe software, a discretization in 100 elements was adopted. This number allows obtaining of smooth displacement shapes, which is specially important for the fluid–structure interaction evaluation, and is within the range where the natural frequencies up to the fifth mode do not depend on further refinements of the mesh, as can be seen in Table 5. The modal shapes are compared in Fig. 4.

Table 4
Natural frequencies (rad/s) obtained for the first five modes of vibration using the Mathematica® eigensystem solver over the PDEs of motion as a function of the maximum element size set for the software (in metres).

Mode	Maximum element size [m]				
	1000	500	100	10	1
1	0.2740	0.2184	0.2000	0.1998	0.1998
2	0.6042	0.3630	0.3172	0.3167	0.3167
3	0.9051	0.5541	0.4441	0.4431	0.4431
4	1.3733	0.8416	0.5575	0.5558	0.5558
5	2.1746	1.1399	0.6791	0.6762	0.6762

Table 5
Natural frequencies (rad/s) obtained for the first five modes of vibration using the Giraffe in-house software as function of the number of elements along the cable length.

Mode	Number of elements				
	10	25	50	100	200
1	0.1984	0.1983	0.1983	0.1983	0.1983
2	0.3150	0.3147	0.3147	0.3147	0.3147
3	0.4419	0.4402	0.4402	0.4402	0.4402
4	0.5570	0.5524	0.5522	0.5522	0.5522
5	0.6838	0.6723	0.6719	0.6719	0.6719

Notice that there is no visible difference between modal shapes obtained with either method and that the relative differences between natural frequencies are all below 1% (see Table 2). Next, the ability of set (iii) to recover the modal shapes is represented in Fig. 5.

It is possible to see that the recovery of the modal shapes is good but not flawless. The effects of those differences can be noticed on the obtained frequencies, as seen in Table 3, with the magnitude of the relative difference largely increasing with the respective error in the recovered modal shape (see the third mode in Fig. 5). It is reasonable then to expect that this difference will induce some discrepancies on the obtained results, which is discussed further on. Notice, however, that the comparisons of time responses are focused on excitations of the first mode. If the third mode would be the interest, further refinement of set(iii) would certainly be necessary.

With the model verified by means of the comparison of the modal properties, the results of simulations can now be addressed. The simulations are carried out during 1000 s, which demonstrated to be enough time for eliminating the initial transitories. The ROMs are integrated with a Runge–Kutta method using the native Matlab® ode45 function. For initial comparisons, an imposed motion of 1 metre (around 5 structural diameters) is considered. In order to shorten the specifications of the analysed ROMs, they are each named as $\text{ROM}_{i,j}$ with i being the number of the projection functions set used (set i, ii or iii) and j is the number of the pair of functions used for the imposed motion interpolation (Eqs. (29) to (34)). Notice that, with the proposed basis, 9 possible different ROMs are defined, combining each of the three sets with each of the three possibilities for imposed motion interpolation. The first comparison is made for $\text{ROMs}_{1,j}$, whose simulations results are presented in Fig. 6 in the form of scalograms.

The results from the FEM simulation (Fig. 6(a)) are not recovered by $\text{ROM}_{1,1}$ or $\text{ROM}_{1,2}$, as can be seen in Figs. 6(b) and 6(c) respectively. The amplitudes are significantly different from the FEM results as well as the shape of the wave pattern presented in the scalograms. In turn, analysing Fig. 6(d), it is possible to say that $\text{ROM}_{1,3}$ leads to results very similar to the FEM solution both in terms of developed amplitudes of motion as well as in the shape of the wave pattern of the displacements along the structure. The results highlight that there are key effects dependent on how the imposed motion is taken into account during the discretization process. For a greater clarity and better quantitative evaluation, the time-series and phase-space portraits for 4 different

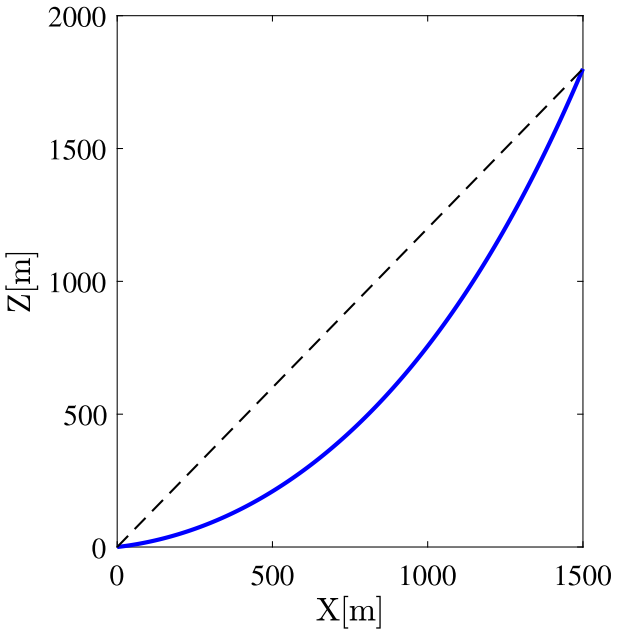

Fig. 3. Calculated static configuration for the data in Table 1.

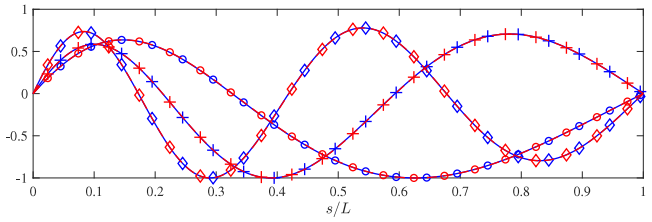

Fig. 4. Comparison between transversal modal shapes obtained by the FEM and a direct application over the PDEs of motion. Blue lines are used for the FEM while red lines are used for the direct solution. First mode indicated by circles, second mode by crosses and third mode by diamonds. (For interpretation of the references to colour in this figure legend, the reader is referred to the web version of this article.)

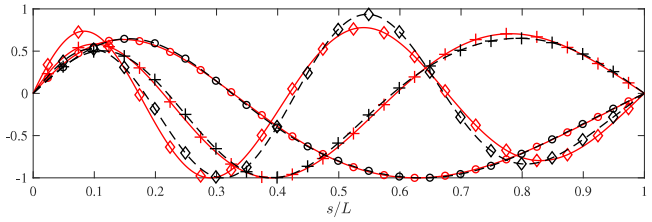

Fig. 5. Comparison between transversal modal shapes obtained by a direct application over the PDEs of motion and the recovery achieved by the trigonometric shape functions of set (iii). Red lines are used for the direct solution while black lines are used for the recovery by trigonometric function. First mode indicated by circles, second mode by crosses and third mode by diamonds. (For interpretation of the references to colour in this figure legend, the reader is referred to the web version of this article.)

Table 6
Comparison between the FEM and $ROM_{1,3}$ results for the maximum amplitude of motion at different cross-sections. Results in metres.

s/L	FEM	$ROM_{1,3}$
0.2	1.5165	1.4452
0.4	1.2470	1.0795
0.6	0.9074	0.9652
0.8	0.5570	0.6801

cross-sections are compared between the FEM and $ROM_{1,3}$ results. This is not made for the other two options since the lack of agreement is already clear by the qualitative correlation shown in Fig. 6. The chosen cross-sections are at s/L values of 0.2, 0.4, 0.6 and 0.8, being presented in Fig. 7.

It is clear that the response along the length is well recovered by $ROM_{1,3}$ based on the results shown in Fig. 7, with some minor differences present. Note also that the frequency is well recovered, with the phase shift between the different responses being due to the very small difference in the frequencies obtained for each model when accumulated along the simulated time. For the sake of comparison, the maximum amplitude at the explored cross sections are shown in Table 6. Complementing the analysis, three snapshots of the structure are shown in Fig. 8. In order to remove the effect of the phase shift between responses, the reference instant of time is took as the one when a peak of the response of the cross-section at $s/L = 0.2$ occurs for each model. The snapshots are then taken at a minimum peak as described, and at instants after it corresponding to 1/8 and 1/4 of the period of the structural response.

As it can be seen from the snapshots in Fig. 8 and from the values in Table 6, the results are in qualitatively good agreement, however some enhancement can still be done.

In order to verify if the results can be enhanced by incrementing the number of functions in the projection basis, Fig. 9 shows the scalograms for the FEM and $ROMs_{2,j}$ solutions.

Again, the ROMs based on the pairs of functions 1 and 2 for the interpolation of the top motion effects are not able to achieve a proper adherence with the taken reference. In Figs. 9(b) and 9(c) it is noticeable that the amplitudes of motion are in a significant disagreement with the reference and the wave pattern, although closer to the reference than $ROM_{1,1}$ and $ROM_{1,2}$, is also quite different. On the other hand, the results in Fig. 9(d) are remarkably adherent to the numerical reference. As made for $ROM_{1,3}$, a set of complementary results are furnished for a clearer analysis. Time-series and phase-space portraits for the same cross-sections already defined, now comparing $ROM_{2,3}$, are presented in Fig. 10. The maximum amplitudes for each cross-section are reported in Table 7, while the snapshots, using the same time instant definition as before, are shown in Fig. 11.

The results show that the enrichment of the projection basis in relation to $ROM_{1,3}$ leads to a significant enhance of the results, with a fine adherence between the time-series results, maximum amplitudes and instantaneous configurations. Notice however that such qualitatively good results are obtained only for the case of the quasi-static approach for the interpolation of the top motion effects. These results show that the choice of projection functions for the Galerkin scheme go beyond a simple necessity of a convergence study on the minimum required number of functions in such basis to achieve the desired accuracy. To highlight that, consider the results in Fig. 12 obtained with $ROMs_{3,j}$.

It is clear that, although the increased number of projection functions leads to better results in terms of amplitudes when using the top motion interpolation sets 1 and 2, the wave pattern is still noticeably different from the reference. One of the main visible indicators for that is the position along the length where the largest displacements occur. While in Figs. 12(b) and 12(c) it is located at $\approx$ 35% of the length of the cable, the reference (Fig. 12(a)) indicates that it should occur at $\approx$ 25% of the length. Analysing now Fig. 12(d), it is possible

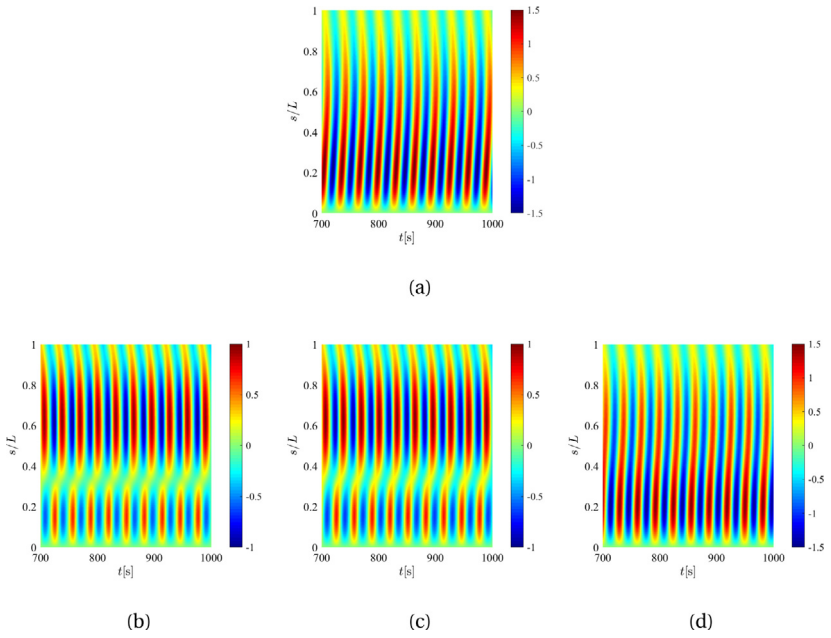

Fig. 6. Scalograms of the transversal response of the structure in steady-state regime. (a) FEM solution. (b) Numerical integration of $ROM_{1,1}$. (c) Numerical integration of $ROM_{1,2}$. (d) Numerical integration of $ROM_{1,3}$.

Table 7
Comparison between the FEM and $ROM_{2,3}$ results for the maximum amplitude of motion at different cross-sections. Results in metres.

s/L	FEM	$ROM_{2,3}$
0.2	1.5165	1.4553
0.4	1.2470	1.2579
0.6	0.9074	0.8998
0.8	0.5570	0.5656

Table 8
Comparison between the FEM and $ROM_{3,3}$ results for the maximum amplitude of motion at different cross-sections. Results in metres.

s/L	FEM	$ROM_{3,3}$
0.2	1.5165	1.4553
0.4	1.2470	1.2579
0.6	0.9074	0.8998
0.8	0.5570	0.5656

to verify a satisfactory accuracy, although the wave pattern obtained is not as adherent to the numerical reference as the one presented in Fig. 9(d). This reassures the observations made regarding the $ROMs_{2,j}$ results, that is, the set of projection functions that are responsible for incorporating the effects of the top motion carries some features that are not recovered by simply adding more functions to the projection basis. Thus, the first conclusion can be drawn: the importance of a careful discussion and selection of the projection functions responsible for taking into account the prescribed motion at the boundary, since a poor selection can lead to inaccurate results and this problem is not solved by simply adding more functions to the remaining set, that obeys the fixed boundary condition. It is also of importance the highlight of the bad recovery that $ROM_{3,3}$ presented for the wave pattern along the cable. In order to further illustrate this flaw, the same types of results presented for the other ROMs are adopted. In Fig. 13, the time-series and phase-space portraits for selected cross-sections are shown, while Table 8 brings the maximum amplitudes obtained for each cross-section in consideration, and Fig. 14 presents the snapshots of instantaneous configurations as already defined.

It is clear that the results using set(iii) presents an spacial incoherence with the dynamics of the problem, even though the maximum amplitudes of motion are obtained with a similar value (however in the wrong position along the cable span). This sets another drawback in the use of simpler functions for the projection basis, since, even with a greater effort using more DOFs, the results are adequate to the reference as expressed by simpler models, such as $ROM_{2,3}$. This highlights yet again the importance of a careful choice of the projection basis. Note also that the vibrations are mainly composed of the top motion effect interpolation function and the first mode of vibration, whose shape was well recovered by the ROMs based on set(iii). This means that, being able to recover modal shapes involved is not always enough to ensure a good quality of the obtained results.

Moving on to further investigations, only ROMs of the form $ROM_{i,3}$ are now considered since the third set of functions for the top motion interpolation is the only one deemed suitable to furnish acceptable results. The spectral content obtained from the FEM simulation and the results furnished by the different ROMs are shown in Figs. 15, 16, 17 and 18.

It is possible to notice that all spectra are concentrated in the region with frequency equal to the natural frequency of the first mode, f_0. This is expected considering that the 1:1 resonance with the first mode was imposed as simulation scenario. Notice however that the spectrum for the FEM simulations has a broad band of contributions in other frequencies that is not present in the simulations using the ROMs. This is likely due to the assumption of a quasi-static approach for dealing with the top motion effects on the structure since it disregards any

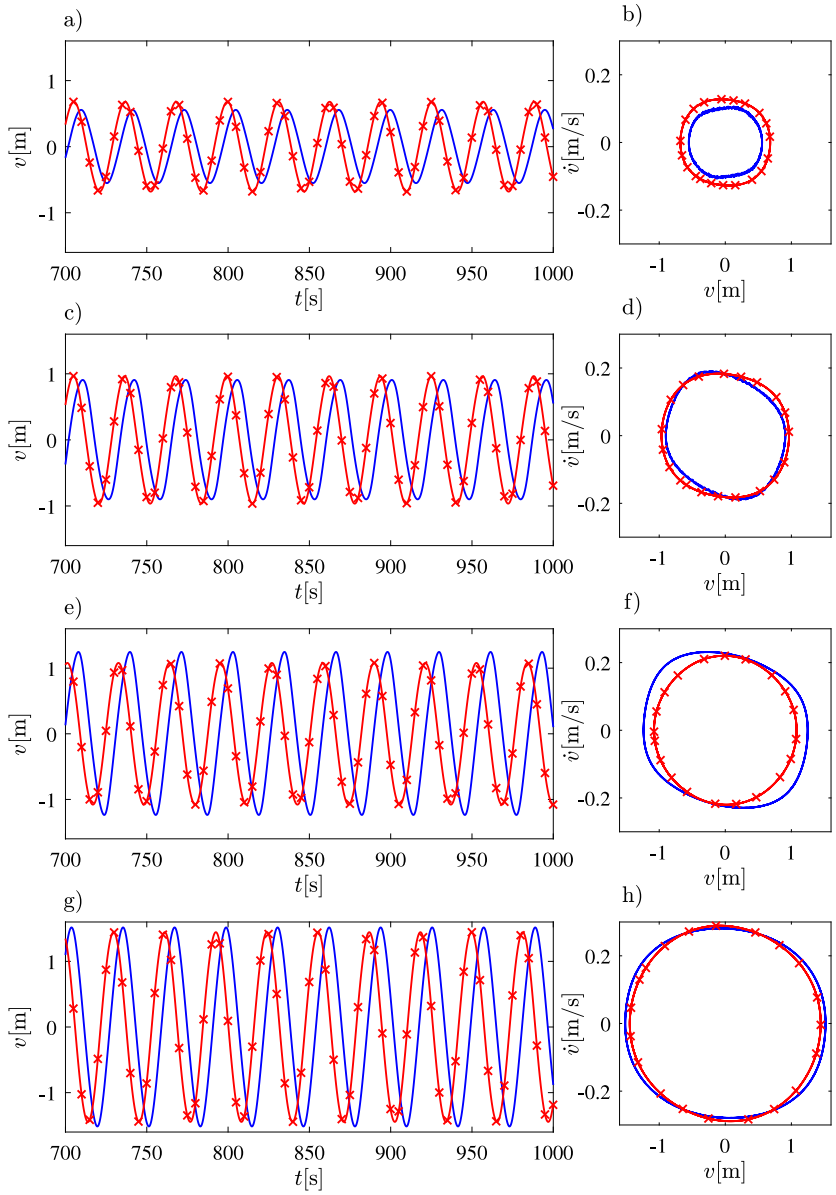

Fig. 7. Time-series and phase-space portraits comparison between $ROM_{1,3}$ (Red lines with crosses markers) and the FEM (blue line without markers) solution for a top motion amplitude of 1 m. (a) Time-series for the cross-section at $s/L = 0.8$. (b) Phase-space portrait for the cross-section at $s/L = 0.8$. (c) Time-series for the cross-section at $s/L = 0.6$. (d) Phase-space portrait for the cross-section at $s/L = 0.6$. (e) Time-series for the cross-section at $s/L = 0.4$. (f) Phase-space portrait for the cross-section at $s/L = 0.4$. (g) Time-series for the cross-section at $s/L = 0.2$. (h) Phase-space portrait for the cross-section at $s/L = 0.2$. (For interpretation of the references to colour in this figure legend, the reader is referred to the web version of this article.)

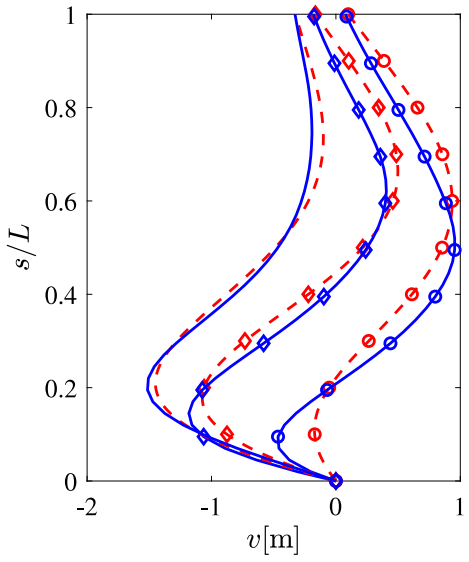

Fig. 8. Snapshots of the structural configuration for a reference instant correspondent to the occurrence of a peak in the response of the cross-section at $s/L = 0.2$ (lines without markers), an instant occurring 1/8 of the period of the structural response (lines with diamond markers) after the reference, and an instant occurring 1/4 of the period of the structural response (lines with diamond markers) after the reference. Comparison between FEM solution (blue continuous line) with $ROM_{1,3}$ (red dashed line). (For interpretation of the references to colour in this figure legend, the reader is referred to the web version of this article.)

the travel time needed for the wave input at the top boundary to reach the lower portions of the cable. This difference however does not significantly impact the accuracy of the obtained results, as shown in the scalograms presented in Figs. 6 to 12.

Following with the analysis, larger amplitudes are now considered for the imposed top motion. Given all the discussion made so far, only the results using the quasi-static interpolation functions are shown, that is, $ROMs_{i,3}$. In Figs. 19, 20, 21 and 22, the results from simulations with 3 m of imposed top motion are shown, while in Figs. 24, 25, 26 and 27 the condition of 5 m of top motion amplitude is used. The results are complemented by time-series and phase-space portraits on selected cross-sections for the ROM with the best results in previous analysis ($ROM_{2,3}$), presented in Fig. 23 for the top motion amplitude of 3 m, and in Fig. 28 for the top motion amplitude of 5 m.

It is possible to notice that all the different ROMs obtain results that are in quite good agreement with the reference, with $ROM_{2,3}$ certainly furnishing the closest result, and with $ROM_{3,3}$ presenting the weakest spacial reconstruction of the desired response, although the maximum displacement is compatible with the reference. It is importance to notice that all ROMs present some difference in wave pattern with respect to the reference, which can be partially credited to the interpolation functions for the top motion. Note also that for $ROM_{2,3}$, the agreement of the displacements along the cable length are in quite good agreement with the reference, even though some small differences may be observed in the scalogram. It is expected that, for larger amplitudes, the results may lose adherence to the reference, requiring a further enrichment of the interpolation set. This is already out of the scope of this work and is left as suggestion for future studies.

Complementing the scalograms shown in Figs. 19 to 27, Fig. 29 shows the maximum transversal response amplitude as a function of the amplitude of the top motion for the different models. It must be kept in mind though that the position where the maximum amplitude occurs is not necessarily the same amongst the different models, with better quality being obtained with $ROM_{1,3}$ and $ROM_{2,3}$. The figure also brings a curve obtained with the MMTS solution with its novel iterative approach presented in this work.

Table 9
Time spent for the numerical simulation of one single scenario for each approach investigated.

Model	Time spent [s]
FEM	744.95
$ROM_{1,3}$	0.14
$ROM_{2,3}$	0.43
$ROM_{3,3}$	8.20

It is possible to see that all ROMs are in good agreement with the reference for all the simulated range of top motion amplitudes, as long as only the maximum value of the amplitude is of concern. Regarding the MMTS solution presented, it is possible to see in Fig. 29 that it closely follows the amplitudes obtained by the ROM it is meant to represent, that is, $ROM_{1,3}$. This shows that the iterative procedure suggested works. However, the necessity of using a numerical iteration scheme brings a drawback to the method, being that it loses the capability of obtaining unstable branches of solution. The tool retains its usefulness in terms of presenting accurate results for the structural response, however, its capability of investigating phenomenons such as bifurcations is hindered. Finally, since the MMTS was applied to the ordinary differential equation that rules $ROM_{1,3}$, all the conclusions drawn for such ROM can be extended to the MMTS solution. This can be done considering that the proposed MMTS solution focuses on the steady-state solution, which is the type of response obtained by the ROM. The advantage is that such amplitude can be computed with the iterative approach with fewer operations than the amount required to integrate the equation of motion until the steady-state regime is achieved. This is particularly useful in cases where a large number of simulations may be required. The iterative process however becomes computationally more expensive than the numerical integration as the number of DOFs is increased, being it interesting only for ROMs with a small number of DOFs. This reinforces the importance of refining the process of generating a ROM, using more detailed projection functions, which leads to smaller ROMs with better accuracy.

Considering that all ROMs presented suitable results in terms of amplitudes, with some points that need attention on the spatial distribution of such amplitude, the question that now rises is if there is one ROM preferable to the others. One way to decide that is to evaluate the computational time needed for the integration of each ROM. This comparison is able to furnish how faster the ROMs are in comparison to the FEM solutions, as well as the expected time for each of them to perform a large number of simulations that may be required in a detailed engineering analysis. To that aim, the simulation times are shown in Table 9. All the simulations where carried out in the same standard microcomputer with a 7th generation i7 processor.

Finally, in order to evaluate the behaviour around the 1:1 resonance, the simplest accurate ROM, that is $ROM_{1,3}$, is used for simulations with some pairs of top motion amplitude and frequency. The results are compared with FEM solutions and are shown in Fig. 30.

It is shown that the ROM is able to maintain adherence to the numerical reference even with variations in the top-motion frequency. With this, it is possible to summarize the conclusions from the present analysis:

- The careful choice of the function responsible for interpolating the effects of the imposed top motion along the structural length is essential for the success of the ROM;
- The choice of projection sets go beyond a simple convergence problem, since, as shown, a larger number of projection functions is not necessarily able to overcome problems identified with selecting a poor function for the top motion interpolation;

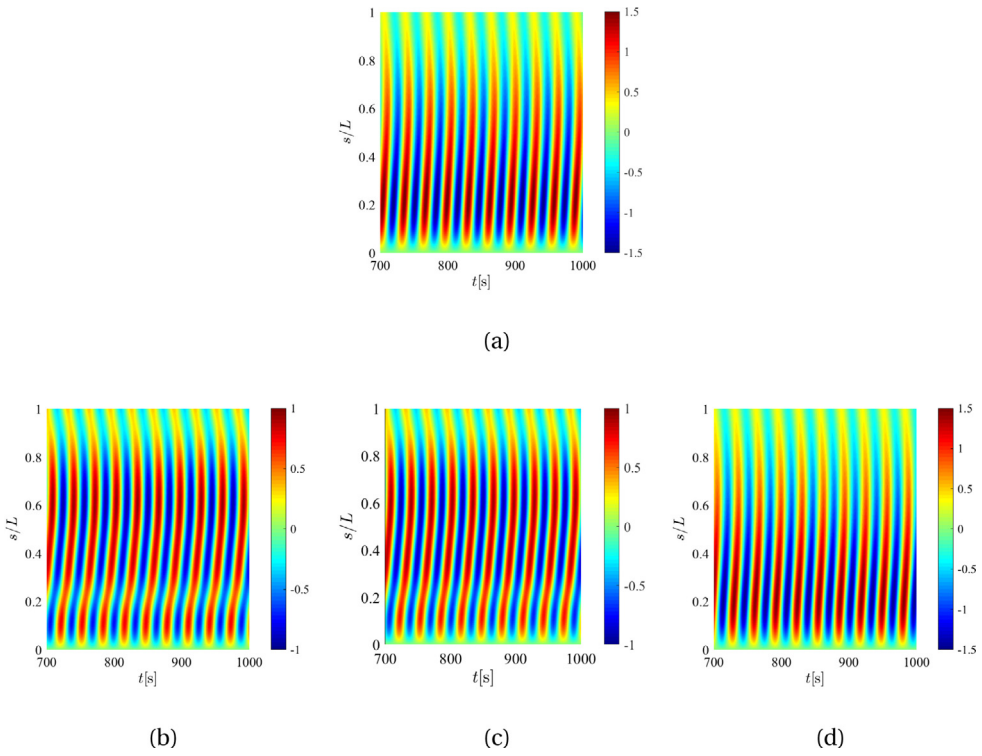

Fig. 9. Scalograms of the transversal response of the structure in steady-state regime. (a) FEM solution. (b) Numerical integration of $ROM_{2,1}$. (c) Numerical integration of $ROM_{2,2}$. (d) Numerical integration of $ROM_{2,3}$.

- Although the actual modes of vibration for this case are more troublesome to work with than trigonometric functions, mostly due to the lack of an analytical expression for them, their use leads to accurate ROM with the use of a smaller number of projections functions. This results in a smaller system to be solved which translates itself into easiness of analysis and lesser computational effort for the same amount of numerical integrations.

6. Final remarks

This work focused on the analysis of the quality of different reduced-order models (ROMs) in order to discuss the advantages of different approaches when conceiving such models as well as aspects that may hinder their accuracy. The problem investigated is that of an elastic cable hanging between two supports, at different heights, immersed in still fluid and subjected to an imposed top motion at one of the supports.

The mathematical modelling of the elastic cable is somewhat new, by writing the equations of motion in a suitable fashion for problems of investigating the dynamics as a perturbation around a static configuration while using a local reference frame in a Lagrangian system. The usual approaches in the literature involve either a Lagrangian approach in Cartesian coordinates or the Eulerian approach. Nine different ROMs were then conceived by combining three possible sets to interpolate the effects of the moving boundary condition with three different sets obtained from the problem with fixed boundaries. This is done in order that the composition of the solution rigorously follows the imposed moving boundary condition in order for the Galerkin method to be properly applied. For the particular case of ROMs with a single degree of freedom (DOF), a novel semi-analytical solution was developed by mixing the method of multiple time scales (MMTS) with a numerical iterative procedure. This is done in order to deal with the absolute value function that appears due to the Morrison damping adopted which do not allow for the computing of the integrals in the Galerkin scheme without knowing the response amplitude.

It is shown that, by means of numerical simulations and comparison with an adopted reference based on the finite element method (FEM), the set of functions chosen to interpolate the effect of the top motion along the structure play an important role in the quality of the results. It is also demonstrated that it is not possible to achieve a good adherence to the desired result by simply adding more projection functions to the ROM depending on the shape adopted for such interpolating functions. This is a novel result showing that the choice of the functions to obtain a ROM deserves a qualitative investigation, going beyond a problem of only numerical convergence. The presented results also show that by enriching the functions on the projection basis, such as using the actual modes of vibration instead of trigonometric functions, allows the use of smaller ROMs which translates itself in smaller computational effort to perform simulations. This can be of topmost importance in conditions where a large number of simulations of the same system are required (for example, in the early stages of design). Another finding is that the spectral compositions of the response of the ROMs are narrow-banded

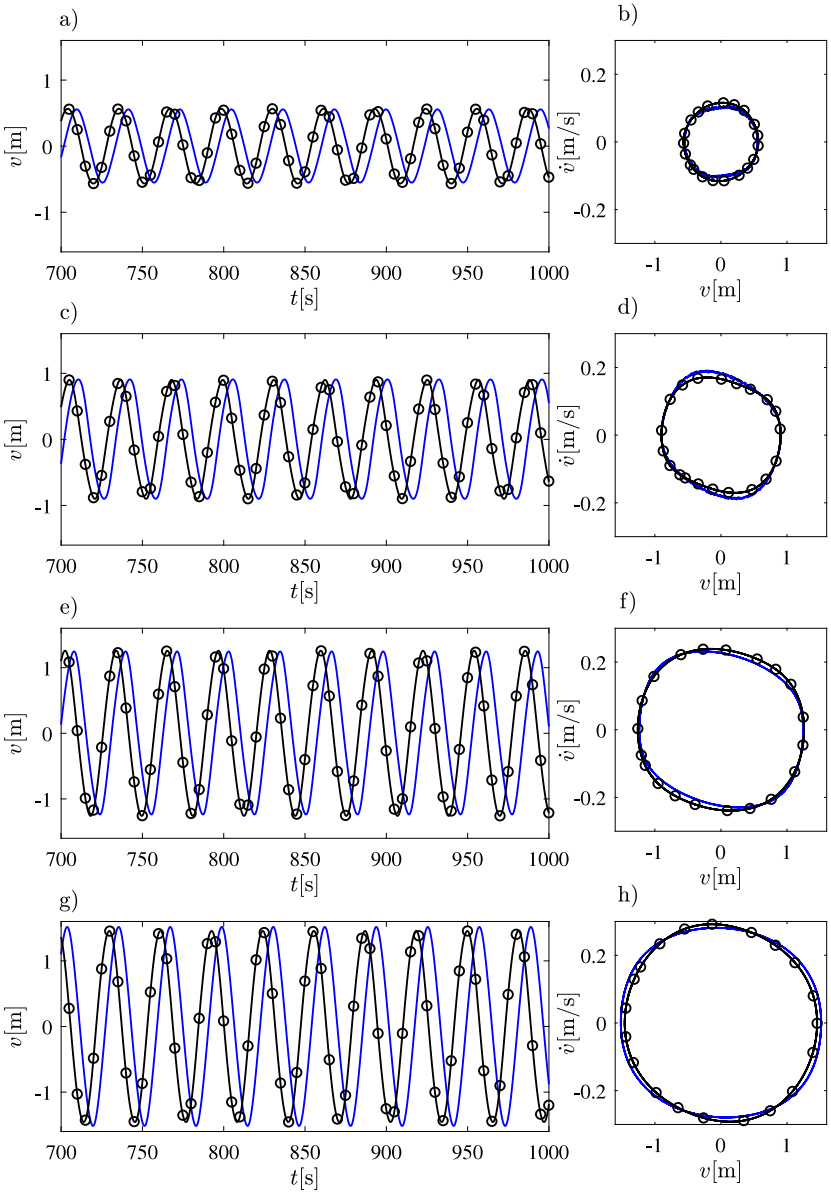

Fig. 10. Time-series and phase-space portraits comparison between $\mathrm{ROM}_{2,3}$ (Black lines with circle markers) and the FEM (blue line without markers) solution for a top motion amplitude of 1 m. (a) Time-series for the cross-section at $s/L = 0.8$. (b) Phase-space portrait for the cross-section at $s/L = 0.8$. (c) Time-series for the cross-section at $s/L = 0.6$. (d) Phase-space portrait for the cross-section at $s/L = 0.6$. (e) Time-series for the cross-section at $s/L = 0.4$. (f) Phase-space portrait for the cross-section at $s/L = 0.4$. (g) Time-series for the cross-section at $s/L = 0.2$. (h) Phase-space portrait for the cross-section at $s/L = 0.2$. (For interpretation of the references to colour in this figure legend, the reader is referred to the web version of this article.)

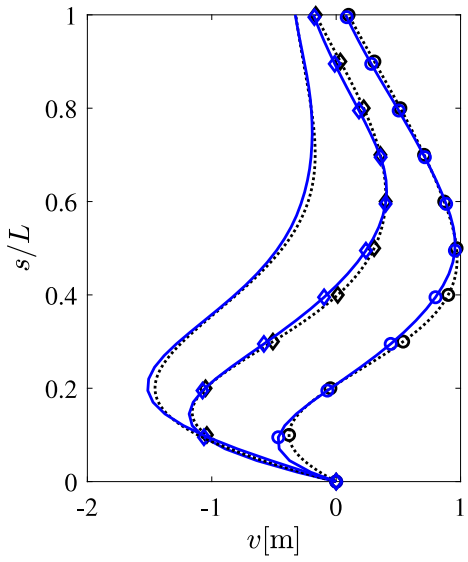

Fig. 11. Snapshots of the structural configuration for a reference instant correspondent to the occurrence of a peak in the response of the cross-section at $s/L = 0.2$ (lines without markers), an instant occurring 1/8 of the period of the structural response (lines with diamond markers) after the reference, and an instant occurring 1/4 of the period of the structural response (lines with diamond markers) after the reference. Comparison between FEM solution (blue continuous line) with $ROM_{2,3}$ (black dotted line). (For interpretation of the references to colour in this figure legend, the reader is referred to the web version of this article.)

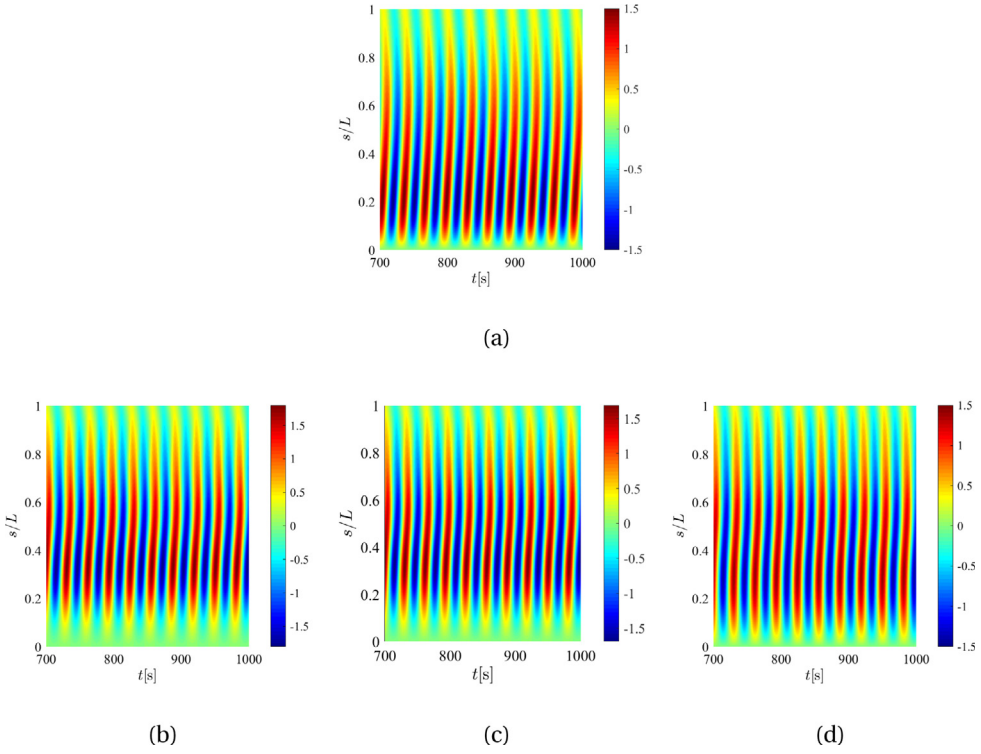

Fig. 12. Scalograms of the transversal response of the structure in steady-state regime. (a) FEM solution. (b) Numerical integration of $ROM_{3,1}$. (c) Numerical integration of $ROM_{3,2}$. (d) Numerical integration of $ROM_{3,3}$.

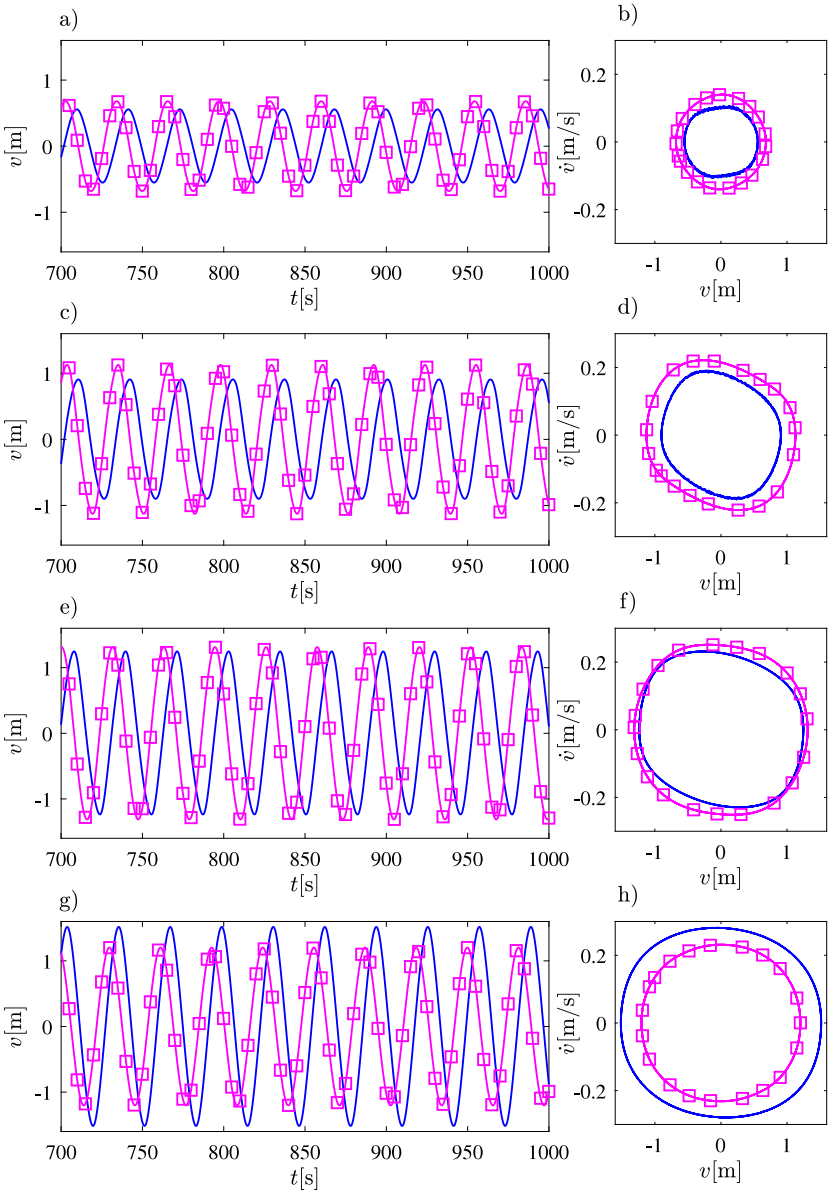

Fig. 13. Time-series and phase-space portraits comparison between $ROM_{3,3}$ (Magenta lines with square markers) and the FEM (blue line without markers) solution for a top motion amplitude of 1 m. (a) Time-series for the cross-section at $s/L = 0.8$. (b) Phase-space portrait for the cross-section at $s/L = 0.8$. (c) Time-series for the cross-section at $s/L = 0.6$. (d) Phase-space portrait for the cross-section at $s/L = 0.6$. (e) Time-series for the cross-section at $s/L = 0.4$. (f) Phase-space portrait for the cross-section at $s/L = 0.4$. (g) Time-series for the cross-section at $s/L = 0.2$. (h) Phase-space portrait for the cross-section at $s/L = 0.2$. (For interpretation of the references to colour in this figure legend, the reader is referred to the web version of this article.)

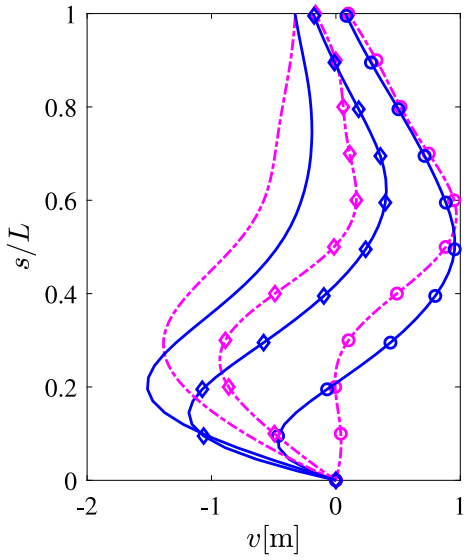

Fig. 14. Snapshots of the structural configuration for a reference instant correspondent to the occurrence of a peak in the response of the cross-section at $s/L = 0.2$ (lines without markers), an instant occurring 1/8 of the period of the structural response (lines with diamond markers) after the reference, and an instant occurring 1/4 of the period of the structural response (lines with diamond markers) after the reference. Comparison between FEM solution (blue continuous line) with $\mathrm{ROM}_{3,3}$ (magenta dash-dot line). (For interpretation of the references to colour in this figure legend, the reader is referred to the web version of this article.)

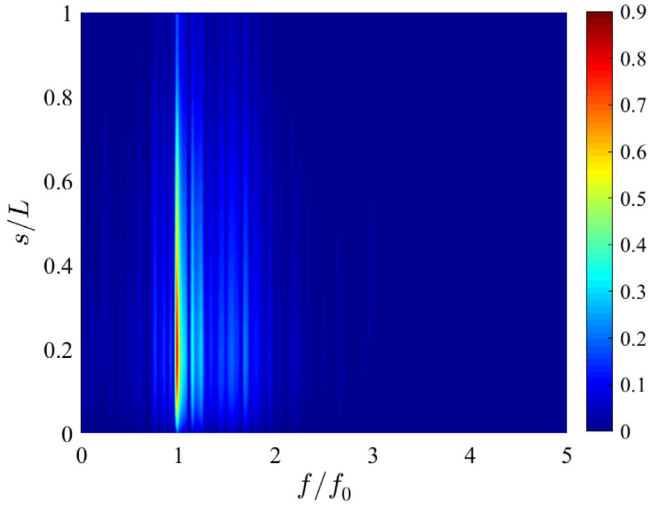

Fig. 15. Spanwise amplitude spectra along the cable length considering the FEM solution for a top motion amplitude of 1 m, with the frequency normalized by the natural frequency of the first vibration mode f_0.

while the FEM solution presents a broad-band of contributions around the investigated resonance frequency. This is likely due to the quasi-static approach considered in the interpolation of the effects of the top motion along the structure.

For further works, three main suggestions are made. First, the problem can be tackled directly over the PDEs by means of the MMTS. Notice that the equations of motion are proposed in this work in a fashion suitable for the task since the dynamics is written as a perturbation over the static configuration. The second suggestion involves the search of a more general function for the top motion interpolation rather than relying on a quasi-static approach. One possible way to tackle the matter is to find a wave solution for this effect that takes into account the travelling time of the effects of the imposed top motion. Finally, the third suggestion is to use the ideas herein exposed

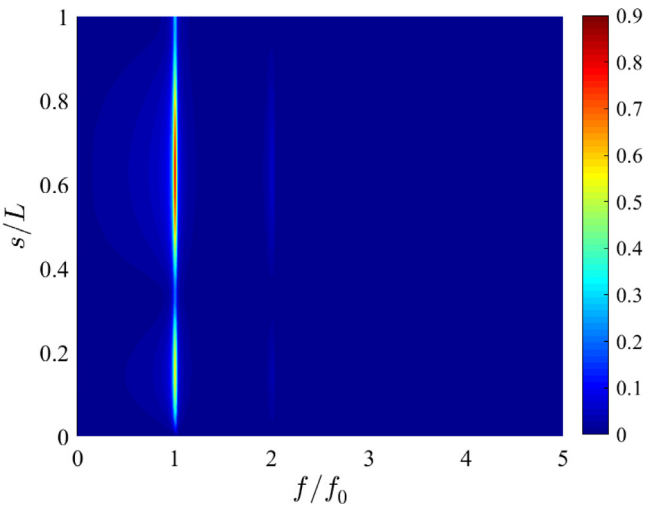

Fig. 16. Spanwise amplitude spectra along the cable length considering the $\mathrm{ROM}_{1,3}$ solution for a top motion amplitude of 1 m, with the frequency normalized by the natural frequency of the first vibration mode f_0.

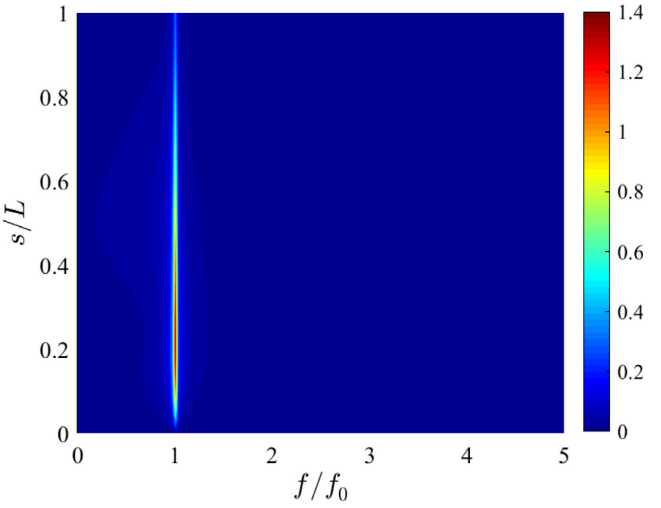

Fig. 17. Spanwise amplitude spectra along the cable length considering the $\mathrm{ROM}_{2,3}$ solution for a top motion amplitude of 1 m, with the frequency normalized by the natural frequency of the first vibration mode f_0.

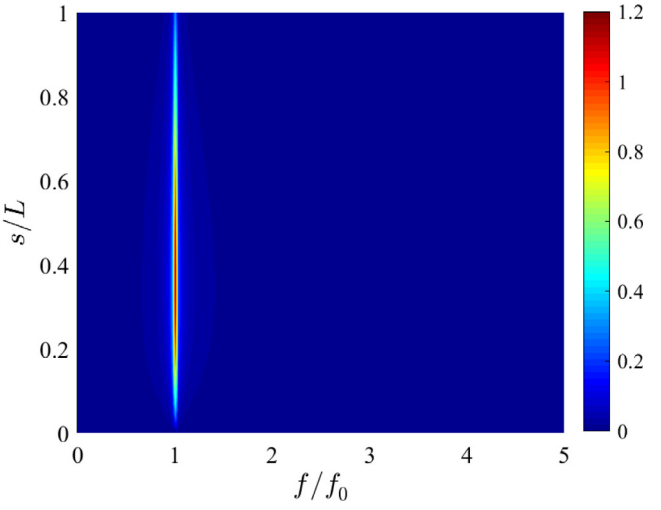

Fig. 18. Spanwise amplitude spectra along the cable length considering the $\mathrm{ROM}_{3,3}$ solution for a top motion amplitude of 1 m, with the frequency normalized by the natural frequency of the first vibration mode f_0.

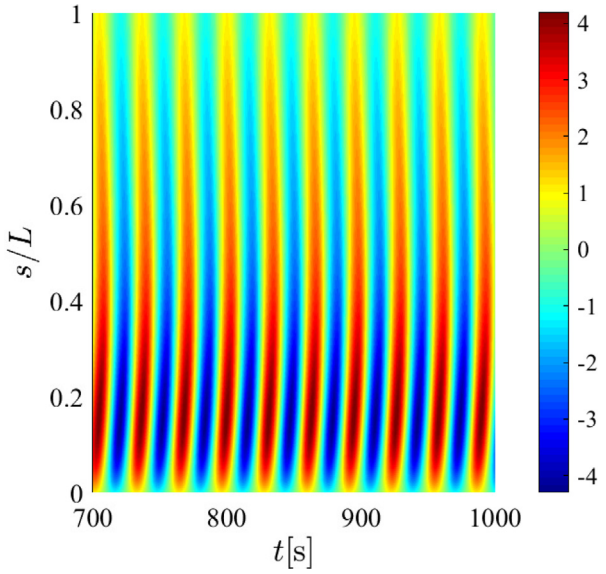

Fig. 19. Scalogram of the transversal response of the structure in steady-state regime considering a top motion amplitude of 3 m, FEM solution.

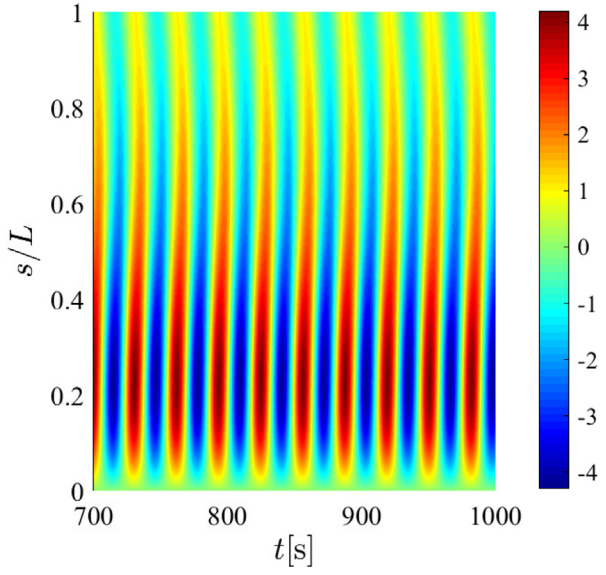

Fig. 20. Scalogram of the transversal response of the structure in steady-state regime considering a top motion amplitude of 3 m, $ROM_{1,3}$ solution.

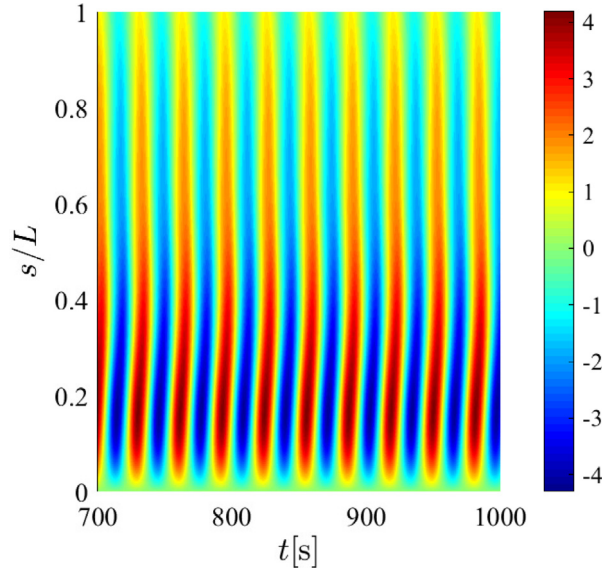

Fig. 21. Scalogram of the transversal response of the structure in steady-state regime considering a top motion amplitude of 3 m, $ROM_{2,3}$ solution.

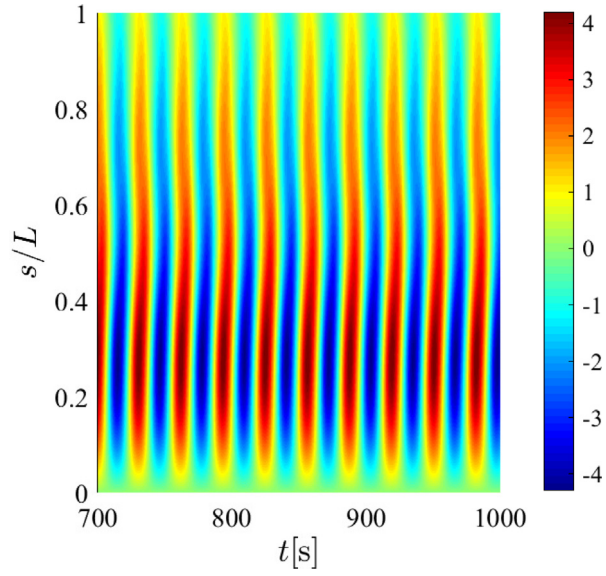

Fig. 22. Scalogram of the transversal response of the structure in steady-state regime considering a top motion amplitude of 3 m, $ROM_{3,3}$ solution.

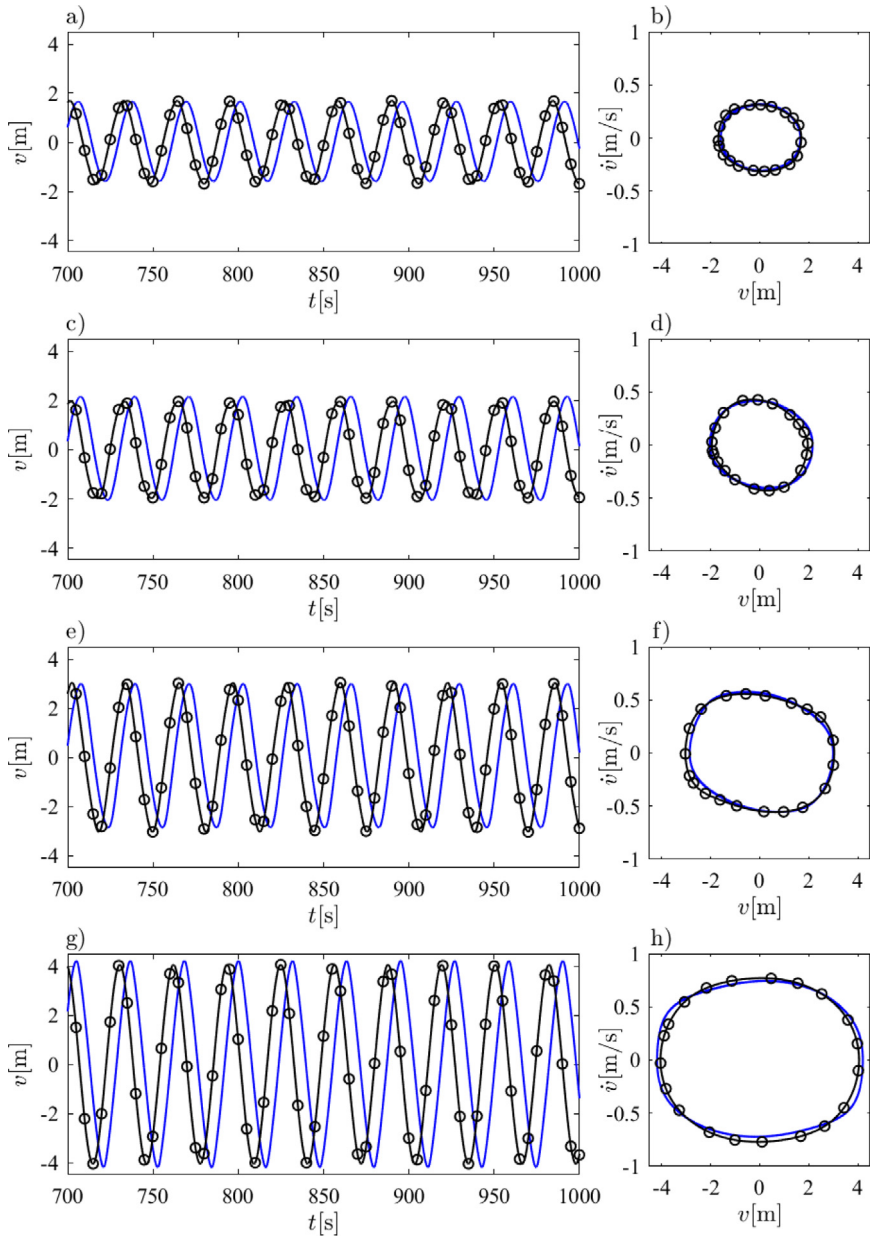

Fig. 23. Time-series and phase-space portraits comparison between $ROM_{2,3}$ (Black lines with circle markers) and the FEM (blue line without markers) solution for a top motion amplitude of 3 m. (a) Time-series for the cross-section at $s/L = 0.8$. (b) Phase-space portrait for the cross-section at $s/L = 0.8$. (c) Time-series for the cross-section at $s/L = 0.6$. (d) Phase-space portrait for the cross-section at $s/L = 0.6$. (e) Time-series for the cross-section at $s/L = 0.4$. (f) Phase-space portrait for the cross-section at $s/L = 0.4$. (g) Time-series for the cross-section at $s/L = 0.2$. (h) Phase-space portrait for the cross-section at $s/L = 0.2$. (For interpretation of the references to colour in this figure legend, the reader is referred to the web version of this article.)

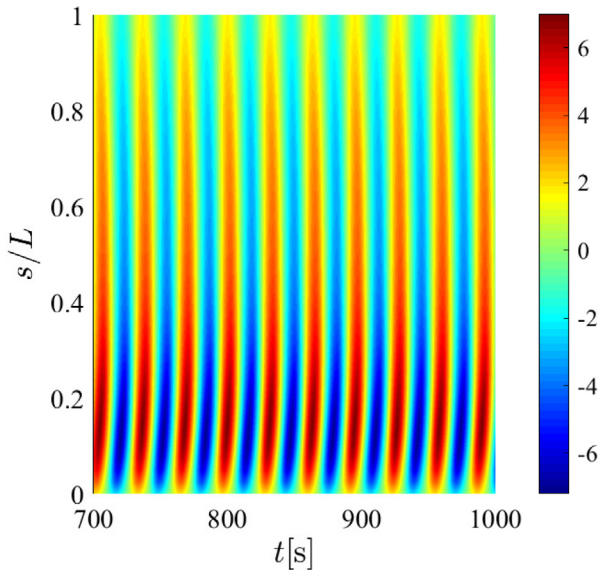

Fig. 24. Scalogram of the transversal response of the structure in steady-state regime considering a top motion amplitude of 5 m, FEM solution.

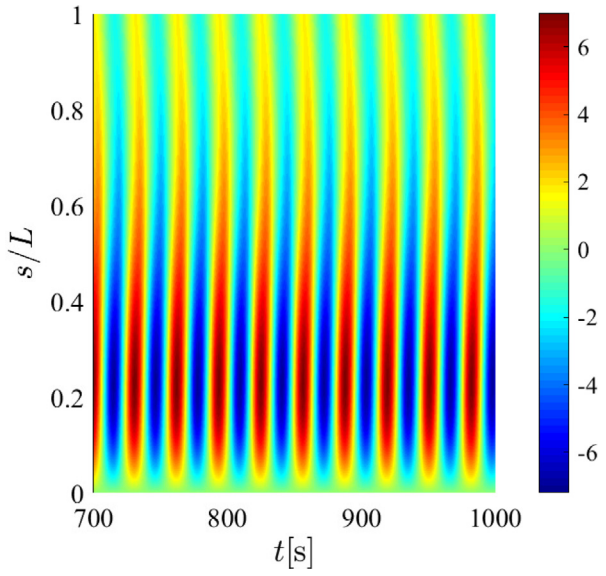

Fig. 25. Scalogram of the transversal response of the structure in steady-state regime considering a top motion amplitude of 5 m, $ROM_{1,3}$ solution.

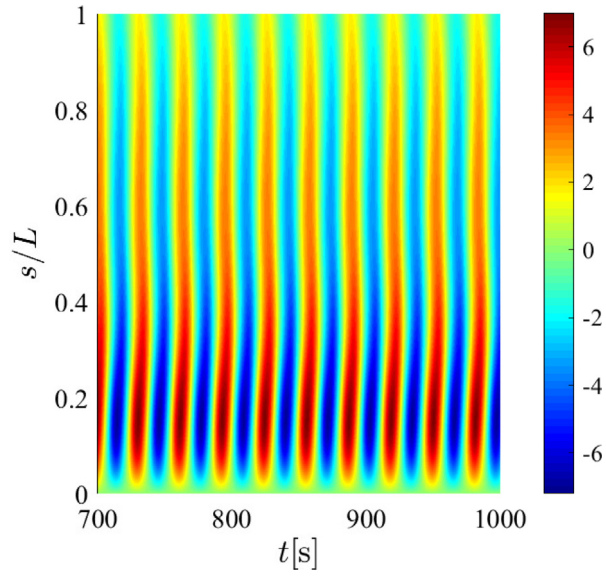

Fig. 26. Scalogram of the transversal response of the structure in steady-state regime considering a top motion amplitude of 5 m, $ROM_{2,3}$ solution.

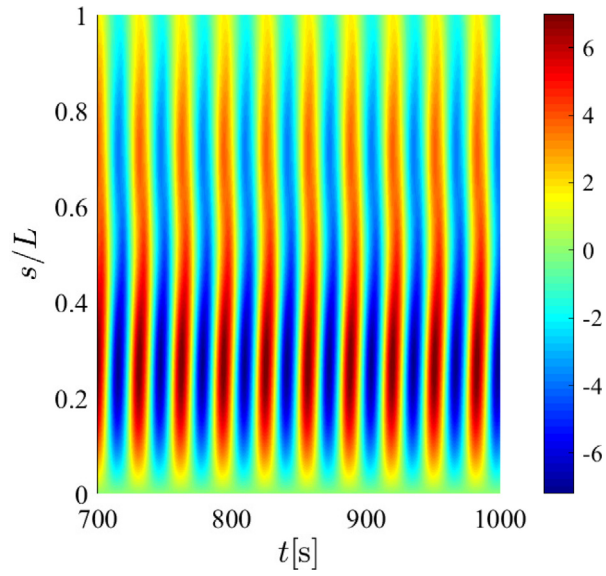

Fig. 27. Scalogram of the transversal response of the structure in steady-state regime considering a top motion amplitude of 5 m, $ROM_{3,3}$ solution.

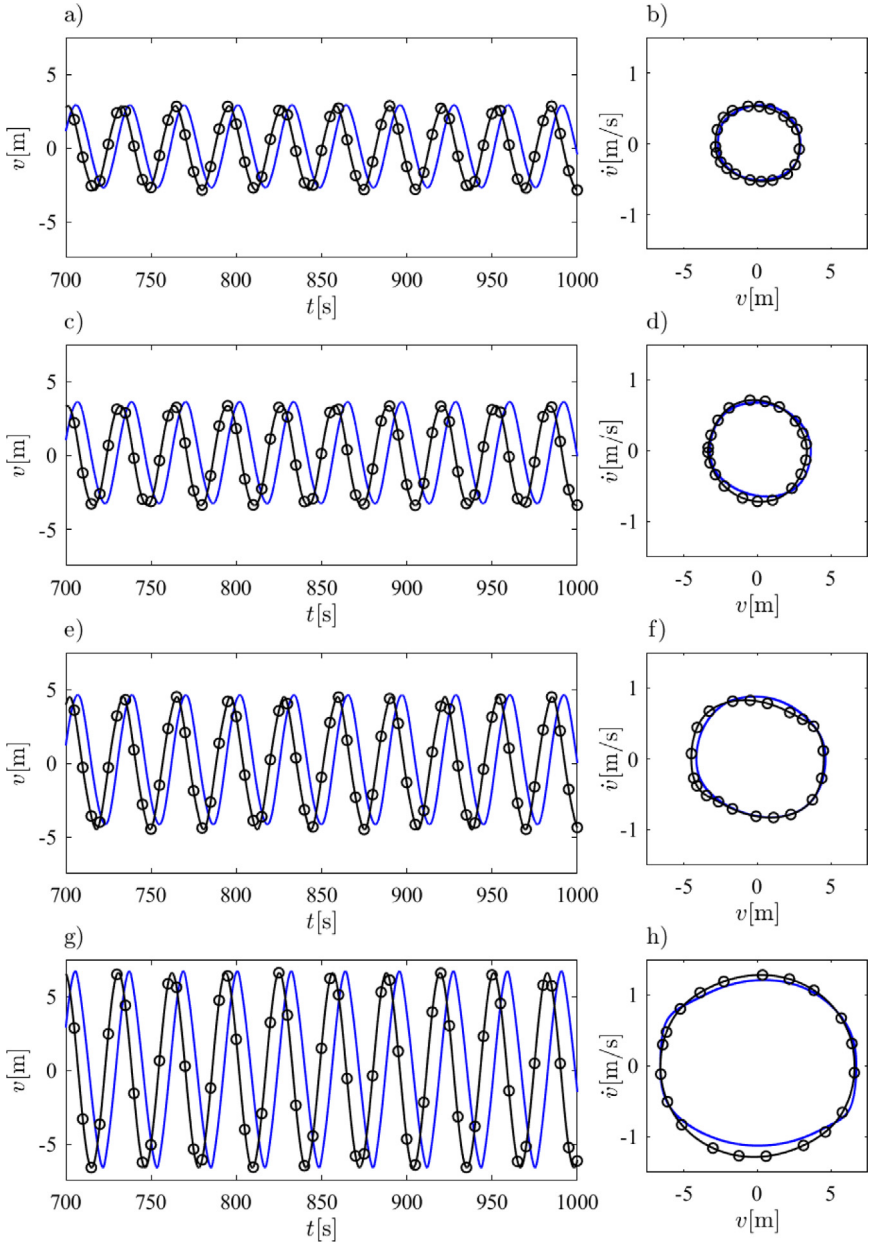

Fig. 28. Time-series and phase-space portraits comparison between $ROM_{2,3}$ (Black lines with circle markers) and the FEM (blue line without markers) solution for a top motion amplitude of 5 m. (a) Time-series for the cross-section at $s/L = 0.8$. (b) Phase-space portrait for the cross-section at $s/L = 0.8$. (c) Time-series for the cross-section at $s/L = 0.6$. (d) Phase-space portrait for the cross-section at $s/L = 0.6$. (e) Time-series for the cross-section at $s/L = 0.4$. (f) Phase-space portrait for the cross-section at $s/L = 0.4$. (g) Time-series for the cross-section at $s/L = 0.2$. (h) Phase-space portrait for the cross-section at $s/L = 0.2$. (For interpretation of the references to colour in this figure legend, the reader is referred to the web version of this article.)

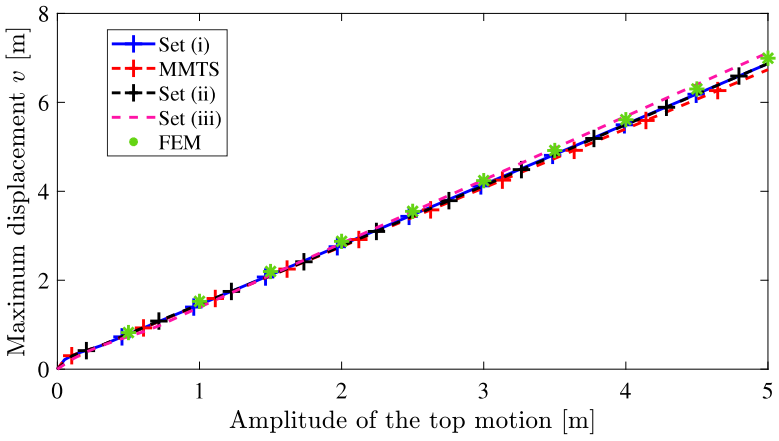

Fig. 29. Comparison of the maximum transversal displacement along the cable length for the case of 1:1 resonance as a function of the imposed motion amplitude. All curves consider the third type of top motion interpolation (quasi-static solution).

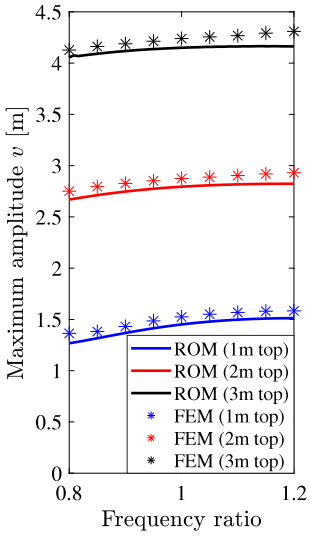

Fig. 30. Comparison of the maximum transversal displacement along the cable length between the FEM and the $ROM_{1,3}$ solutions as a function of the imposed motion frequency for three different top motion amplitudes.

for obtaining an automated software capable of generating the ROMs following the presented guidelines and performing the large number of simulations required for problems such as determining basins of attraction or performing design optimization.

CRediT authorship contribution statement

Guilherme Jorge Vernizzi: Conceptualization, Methodology, Software, Formal analysis, Writing – original draft. **Stefano Lenci:** Conceptualization, Methodology, Writing – original draft, Supervision. **Guilherme Rosa Franzini:** Conceptualization, Methodology, Writing – original draft, Supervision.

Declaration of competing interest

The authors declare that they have no known competing financial interests or personal relationships that could have appeared to influence the work reported in this paper.

Acknowledgements

The first author acknowledges the São Paulo Research Foundation (FAPESP) for research grants n. 2016/25457-1 and 2017/16578-2. The third author thanks the Brazilian Research Council (CNPq) for the grant 305945/2020-3. The PhD candidate Vitor Schwenck Franco Maciel from the Offshore Mechanics Laboratory (LMO - USP) is also acknowledged for his valuable help in the elaboration of Figs. 1 and 2.

References

[1] S. Chucheepsakul, T. Monprapussorn, T. Huang, Large strain formulations of extensible flexible marine pipes transporting fluid, J. Fluids Struct. 17 (2) (2003) 185–224, http://dx.doi.org/10.1016/s0889-9746(02)00116-0.
[2] G. Rega, Nonlinear vibrations of suspended cables–Part I: Modeling and analysis, Appl. Mech. Rev. 57 (6) (2004) 443–478, http://dx.doi.org/10.1115/1.1777224.
[3] H.M. Irvine, T.K. Caughey, The linear theory of free vibrations of a suspended cable, Proc. Royal Soc. 341 (1974) 299–315.
[4] M. Irvine, Cable Structures, MIT Press, Cambridge, 1981.
[5] M. Gambhir, B. deV. Batchelor, Parametric study of free vibration of sagged cables, Comput. Struct. 8 (5) (1978) 641–648, http://dx.doi.org/10.1016/0045-7949(78)90102-5.
[6] G. Rega, A. Luongo, Natural vibrations of suspended cables with flexible supports, Comput. Struct. 12 (1) (1980) 65–75, http://dx.doi.org/10.1016/0045-7949(80)90094-2.
[7] M.S. Triantafyllou, The dynamics of taut inclined cables, Quart. J. Mech. Appl. Math. 37 (3) (1984) 421–440, http://dx.doi.org/10.1093/qjmam/37.3.421.
[8] M.S. Triantafyllou, L. Grinfogel, Natural frequencies and modes of inclined cables, J. Struct. Eng. 112 (1) (1986) 139–148, http://dx.doi.org/10.1061/(asce)0733-9445(1986)112:1(139).
[9] J.C. Russell, T.J. Lardner, Experimental determination of frequencies and tension for elastic cables, J. Eng. Mech. 124 (10) (1998) 1067–1072, http://dx.doi.org/10.1061/(asce)0733-9399(1998)124:10(1067).
[10] P. Hagedorn, B. Schäfer, On non-linear free vibrations of an elastic cable, Int. J. Non-Linear Mech. 15 (4–5) (1980) 333–340, http://dx.doi.org/10.1016/0020-7462(80)90018-9.
[11] A. Luongo, G. Rega, F. Vestroni, Monofrequent oscillations of a non-linear model of a suspended cable, J. Sound Vib. 82 (2) (1982) 247–259, http://dx.doi.org/10.1016/0022-460x(82)90533-8.
[12] G. Rega, F. Vestroni, F. Benedettini, Parametric analysis of large amplitude free vibrations of a suspended cable, Int. J. Solids Struct. 20 (2) (1984) 95–105, http://dx.doi.org/10.1016/0020-7683(84)90001-5.
[13] F. Benedettini, G. Rega, F. Vestroni, Modal coupling in the free nonplanar finite motion of an elastic cable, Meccanica 21 (1) (1986) 38–46, http://dx.doi.org/10.1007/bf01556315.
[14] F. Benedettini, G. Rega, Planar non-linear oscillations of elastic cables under superharmonic resonance conditions, J. Sound Vib. 132 (3) (1989) 353–366, http://dx.doi.org/10.1016/0022-460x(89)90630-5.
[15] G. Rega, F. Benedettini, Planar non-linear oscillations of elastic cables under subharmonic resonance conditions, J. Sound Vib. 132 (3) (1989) 367–381, http://dx.doi.org/10.1016/0022-460x(89)90631-7.
[16] C.P. Pesce, A.L.C. Fujarra, A.N. Simos, E.A. Tannuri, Analytical and closed form solutions for deep water riser-like eigenvalue problem, in: Proceedings of the Ninth (9th) International Offshore and Polar Engineering Conference, 1999.

[17] C.M. Bender, S.A. Orszag, Advanced Mathematical Methods for Scientists and Engineers, McGraw-Hill, 1978.
[18] N. Srinil, G. Rega, S. Chucheepsakul, Large amplitude three-dimensional free vibrations of inclined sagged elastic cables, Nonlinear Dynam. 33 (2) (2003) 129–154, http://dx.doi.org/10.1023/a:1026019222997.
[19] N. Srinil, G. Rega, S. Chucheepsakul, Three-dimensional non-linear coupling and dynamic tension in the large-amplitude free vibrations of arbitrarily sagged cables, J. Sound Vib. 269 (3–5) (2004) 823–852, http://dx.doi.org/10.1016/s0022-460x(03)00137-8.
[20] N. Srinil, G. Rega, S. Chucheepsakul, Two-to-one resonant multi-modal dynamics of horizontal/inclined cables. Part I: Theoretical formulation and model validation, Nonlinear Dynam. 48 (3) (2006) 231–252, http://dx.doi.org/10.1007/s11071-006-9086-0.
[21] N. Srinil, G. Rega, Two-to-one resonant multi-modal dynamics of horizontal/inclined cables. Part II: Internal resonance activation, reduced-order models and nonlinear normal modes, Nonlinear Dynam. 48 (3) (2006) 253–274, http://dx.doi.org/10.1007/s11071-006-9087-z.
[22] X. Zhou, S. Yan, F. Chu, In-plane free vibrations of an inclined taut cable, J. Vib. Acoust. 133 (3) (2011) 031001, http://dx.doi.org/10.1115/1.4003397.
[23] W. Lacarbonara, A. Paolone, F. Vestroni, Elastodynamics of nonshallow suspended cables: Linear modal properties, J. Vib. Acoust. 129 (4) (2007) 425, http://dx.doi.org/10.1115/1.2748463.
[24] A. Mansour, O.B. Mekki, S. Montassar, G. Rega, Catenary-induced geometric nonlinearity effects on cable linear vibrations, J. Sound Vib. 413 (2018) 332–353, http://dx.doi.org/10.1016/j.jsv.2017.10.012.
[25] G.J. Vernizzi, G.R. Franzini, C.P. Pesce, Non-linear free vibrations of a hanging cable with small sag, in: IUTAM Symposium on Exploiting Nonlinear Dynamics for Engineering Systems, Springer International Publishing, 2019, pp. 261–270, http://dx.doi.org/10.1007/978-3-030-23692-2_23.
[26] N. Perkins, Modal interactions in the non-linear response of elastic cables under parametric/external excitation, Int. J. Non-Linear Mech. 27 (2) (1992) 233–250, http://dx.doi.org/10.1016/0020-7462(92)90083-j.
[27] F. Benedettini, G. Rega, R. Alaggio, Non-linear oscillations of a four-degree-of-freedom model of a suspended cable under multiple internal resonance conditions, J. Sound Vib. 182 (5) (1995) 775–798, http://dx.doi.org/10.1006/jsvi.1995.0232.
[28] M. El-Attar, A. Ghobarah, T. Aziz, Non-linear cable response to multiple support periodic excitation, Eng. Struct. 22 (10) (2000) 1301–1312, http://dx.doi.org/10.1016/s0141-0296(99)00065-6.
[29] G. Rega, R. Alaggio, F. Benedettini, Experimental investigation of the nonlinear response of a hanging cable. Part I. Local analysis, Nonlinear Dynam. 14 (2) (1997) 89–117, http://dx.doi.org/10.1023/a:1008246504104.
[30] H. Chen, D. Zuo, Z. Zhang, Q. Xu, Bifurcations and chaotic dynamics in suspended cables under simultaneous parametric and external excitations, Nonlinear Dynam. 62 (3) (2010) 623–646, http://dx.doi.org/10.1007/s11071-010-9750-2.
[31] T. Guo, H. Kang, L. Wang, Y. Zhao, A boundary modulation formulation for cable's non-planar coupled dynamics under out-of-plane support motion, Arch. Appl. Mech. 86 (4) (2015) 729–741, http://dx.doi.org/10.1007/s00419-015-1058-8.
[32] T. Guo, H. Kang, L. Wang, Y. Zhao, Cable's mode interactions under vertical support motions: boundary resonant modulation, Nonlinear Dynam. 84 (3) (2015) 1259–1279, http://dx.doi.org/10.1007/s11071-015-2565-4.
[33] T. Guo, H. Kang, L. Wang, Y. Zhao, Cable dynamics under non-ideal support excitations: Nonlinear dynamic interactions and asymptotic modelling, J. Sound Vib. 384 (2016) 253–272, http://dx.doi.org/10.1016/j.jsv.2016.08.020.
[34] T. Guo, H. Kang, L. Wang, Y. Zhao, Cable's non-planar coupled vibrations under asynchronous out-of-plane support motions: travelling wave effect, Arch. Appl. Mech. 86 (9) (2016) 1647–1663, http://dx.doi.org/10.1007/s00419-016-1141-9.
[35] T. Guo, H. Kang, L. Wang, Y. Zhao, An investigation into cables' in-plane dynamics under multiple support motions using a boundary modulation approach, Arch. Appl. Mech. 87 (6) (2017) 989–1006, http://dx.doi.org/10.1007/s00419-017-1226-0.
[36] J. Warminski, D. Zulli, G. Rega, J. Latalski, Revisited modelling and multimodal nonlinear oscillations of a sagged cable under support motion, Meccanica 51 (11) (2016) 2541–2575, http://dx.doi.org/10.1007/s11012-016-0450-y.
[37] S.A. Nayfeh, A.H. Nayfeh, D.T. Mook, Nonlinear response of a taut string to longitudinal and transverse end excitation, J. Vib. Control 1 (3) (1995) 307–334, http://dx.doi.org/10.1177/107754639500100304.
[38] A. Berlioz, C.-H. Lamarque, A non-linear model for the dynamics of an inclined cable, J. Sound Vib. 279 (3–5) (2005) 619–639, http://dx.doi.org/10.1016/j.jsv.2003.11.069.
[39] L. Wang, Y. Zhao, Large amplitude motion mechanism and non-planar vibration character of stay cables subject to the support motions, J. Sound Vib. 327 (1–2) (2009) 121–133, http://dx.doi.org/10.1016/j.jsv.2009.06.013.
[40] A. Gonzalez-Buelga, S. Neild, D. Wagg, J. Macdonald, Modal stability of inclined cables subjected to vertical support excitation, J. Sound Vib. 318 (3) (2008) 565–579, http://dx.doi.org/10.1016/j.jsv.2008.04.031.
[41] J. Macdonald, M. Dietz, S. Neild, A. Gonzalez-Buelga, A. Crewe, D. Wagg, Generalised modal stability of inclined cables subjected to support excitations, J. Sound Vib. 329 (21) (2010) 4515–4533, http://dx.doi.org/10.1016/j.jsv.2010.05.002.
[42] J. Macdonald, Multi-modal vibration amplitudes of taut inclined cables due to direct and/or parametric excitation, J. Sound Vib. 363 (2016) 473–494, http://dx.doi.org/10.1016/j.jsv.2015.11.012.
[43] A. Luongo, D. Zulli, Dynamic instability of inclined cables under combined wind flow and support motion, Nonlinear Dynam. 67 (1) (2011) 71–87, http://dx.doi.org/10.1007/s11071-011-9958-9.
[44] F.K. Alfosail, M.I. Younis, Two-to-one internal resonance of an inclined marine riser under harmonic excitations, Nonlinear Dynam. 95 (2) (2018) 1301–1321, http://dx.doi.org/10.1007/s11071-018-4630-2.
[45] F.K. Alfosail, M.I. Younis, Three-to-one internal resonance of inclined marine riser, Int. J. Non-Linear Mech. 109 (2019) 107–117, http://dx.doi.org/10.1016/j.ijnonlinmec.2018.11.008.
[46] F.K. Alfosail, M.I. Younis, Multifrequency excitation of an inclined marine riser under internal resonances, Nonlinear Dynam. 99 (2020) 149–171, http://dx.doi.org/10.1007/s11071-019-05136-w.
[47] I. Chatjigeorgiou, On the parametric excitation of vertical elastic slender structures and the effect of damping in marine applications, Appl. Ocean Res. 26 (1–2) (2004) 23–33, http://dx.doi.org/10.1016/j.apor.2004.08.001.
[48] G.J. Vernizzi, G.R. Franzini, S. Lenci, Reduced-order models for the analysis of a vertical rod under parametric excitation, Int. J. Mech. Sci. 163 (2019) 105122, http://dx.doi.org/10.1016/j.ijmecsci.2019.105122.
[49] G.J. Vernizzi, S. Lenci, G.R. Franzini, A detailed study of the parametric excitation of a vertical heavy rod using the method of multiple scales, Meccanica 55 (12) (2020) 2423–2437, http://dx.doi.org/10.1007/s11012-020-01247-6.
[50] G. Rega, W. Lacarbonara, A. Nayfeh, C. Chin, Multiple resonances in suspended cables: Direct versus reduced-order models, Int. J. Non-Linear Mech. 34 (5) (1999) 901–924, http://dx.doi.org/10.1016/s0020-7462(98)00065-1.
[51] T. Guo, G. Rega, H. Kang, L. Wang, Two perturbation formulations of the nonlinear dynamics of a cable excited by a boundary motion, Appl. Math. Model. 79 (2020) 434–450, http://dx.doi.org/10.1016/j.apm.2019.10.045.
[52] G. Kerschen, J. claude Golinval, A.F. Vakakis, L.A. Bergman, The method of proper orthogonal decomposition for dynamical characterization and order reduction of mechanical systems: An overview, Nonlinear Dynam. 41 (1–3) (2005) 147–169, http://dx.doi.org/10.1007/s11071-005-2803-2.
[53] S.W. Shaw, C. Pierre, Normal modes for non-linear vibratory systems, J. Sound Vib. 164 (1993) 85–124.
[54] E. Pesheck, C. Pierre, S. Shaw, A new Galerkin-based approach for accurate non-linear normal modes through invariant manifolds, J. Sound Vib. 249 (5) (2002) 971–993, http://dx.doi.org/10.1006/jsvi.2001.3914.
[55] A.H. Nayfeh, S.A. Nayfeh, On nonlinear modes of continuous systems, J. Vib. Acoust. 116 (1) (1994) 129–136, http://dx.doi.org/10.1115/1.2930388.
[56] G. Kerschen, M. Peeters, J. Golinval, A. Vakakis, Nonlinear normal modes, Part I: A useful framework for the structural dynamicist, Mech. Syst. Signal Process. 23 (1) (2009) 170–194, http://dx.doi.org/10.1016/j.ymssp.2008.04.002.
[57] M. Peeters, R. Viguié, G. Sérandour, G. Kerschen, J.-C. Golinval, Nonlinear normal modes, Part II: Toward a practical computation using numerical continuation techniques, Mech. Syst. Signal Process. 23 (1) (2009) 195–216, http://dx.doi.org/10.1016/j.ymssp.2008.04.003.
[58] C.E. Mazzilli, P.B. Gonçalves, G.R. Franzini, Reduced-order modelling based on non-linear modes, Int. J. Mech. Sci. 214 (2022) 106915, http://dx.doi.org/10.1016/j.ijmecsci.2021.106915.
[59] G. Haller, S. Ponsioen, Nonlinear normal modes and spectral submanifolds: existence, uniqueness and use in model reduction, Nonlinear Dynam. 86 (3) (2016) 1493–1534, http://dx.doi.org/10.1007/s11071-016-2974-z.
[60] S. Ponsioen, S. Jain, G. Haller, Model reduction to spectral submanifolds and forced-response calculation in high-dimensional mechanical systems, J. Sound Vib. 488 (2020) 115640, http://dx.doi.org/10.1016/j.jsv.2020.115640.
[61] O.M. O'Reilly, Modeling Nonlinear Problems in the Mechanics of Strings and Rods, Springer International Publishing, 2017, http://dx.doi.org/10.1007/978-3-319-50598-5.
[62] A.H. Nayfeh, D.T. Mook, Nonlinear Oscillations, John Wiley & Sons, 1979.
[63] A.G. Neto, Giraffe user's manual - generic interface readily accessible for finite elements, 2021, URL http://sites.poli.usp.br/p/alfredo.gay/giraffe/GIRAFFE_Manual.pdf.
[64] A.G. Neto, C.A. Martins, P.M. Pimenta, Static analysis of offshore risers with a geometrically-exact 3D beam model subjected to unilateral contact, Comput. Mech. 53 (1) (2013) 125–145, http://dx.doi.org/10.1007/s00466-013-0897-9.
[65] A.G. Neto, Dynamics of offshore risers using a geometrically-exact beam model with hydrodynamic loads and contact with the seabed, Eng. Struct. 125 (2016) 438–454, http://dx.doi.org/10.1016/j.engstruct.2016.07.005.